DALTON
FULL PAPER

Synthesis and characterization of dinuclear complexes of 3,3′,4,4′-tetraminobiphenyl with tetramminoruthenium and bis(bipyridine)-ruthenium residues and their two- and four-electron oxidized products including a ZINDO study of orbital mixing as a function of ligand oxidation state †

Robert A. Metcalfe,‡[a] Luiz C. G. Vasconcellos,§[b] Hameed Mirza,[a] Douglas W. Franco *[b] and A. B. P. Lever *[a]

[a] *Department of Chemistry, York University, 4700 Keele Street, Toronto, Ontario, Canada, M3J 1P3*
[b] *Department of Chemistry, Universidade de São Paulo, Instituto Física e Química de São Carlos, Av. Dr. Carlos Botelho, 1465, Cx. P. 780- CEP 13560-907, São Carlos, SP, Brasil*

Received 12th April 1999, Accepted 21st June 1999

This paper reports the synthesis, characterisation and reactivity of new complexes of ruthenium, the symmetric dinuclear complex of ruthenium tetrammine $[(Ru(NH_3)_4)_2(catH_4{\cdot}catH_4)](PF_6)_4$ and the asymmetric dinuclear complex of ruthenium bis(bipyridine) and ruthenium tetrammine $[Ru(NH_3)_4(catH_4{\cdot}catH_4)Ru(bpy)_2](PF_6)_4$ where $(catH_4{\cdot}catH_4)$ represents the bridging ligand 3,3′,4,4′-tetraminobiphenyl. These complexes can be oxidized to the two-electron oxidized ligand mixed valence $(qH_2{\cdot}catH_4)$ species and the four-electron oxidized ligand $(qH_2{\cdot}qH_2)$ species. Further oxidation yields a range of Ru(III) species. These complexes were studied by proton NMR, UV–VIS spectra, cyclic voltammetry and ZINDO/1 and ZINDO/S calculations.

Introduction

Recent work in this laboratory has focussed on the extensive mixing that exists between the metal d orbitals of $[Ru(bpy)_2]^{2+}$ and $[Ru(NH_3)_4]^{2+}$ fragments, (bpy = 2,2′-bipyridine) and the molecular orbitals of a series of dioxolene, *o*-phenylenediamine (opda), aminothiophenolate and *o*-benzoquinonediimine (bqdi) ligands.[1–5] The extent of mixing can be altered by changing the oxidation state of the ligand. Two major objectives are: (i) a greater understanding of the electronic nature of strongly coupled metal–ligand systems and (ii) the construction of polymeric versions of these complexes that may be used as molecular wires, which could be switched by altering the oxidation state of the metal or the bridging ligand. The polymeric versions of these complexes will be capable of forming mixed valence species, not only involving the two metal centres, but also within the ligand itself.

The neutral 3,3′,4,4′-tetraminobiphenyl (Fig. 1), abbreviated as $(catH_4{\cdot}catH_4)$, contains two *o*-phenylenediamine groups that are bonded together. Each end can be oxidized, in principle independently, to the semiquinonediimine (sqH_2) with loss of two protons from each segment (one-electron–two-proton loss per fragment) and then each fragment can be oxidized by one electron to the quinonediimine oxidation state, the neutral qH_2.[1–6] The H_n subscript number indicates the number of NH protons in each fragment of the molecule.

This ligand has been used previously as a first step towards the synthesis and understanding of a polymeric version of the dioxolene or *o*-phenylenediamine type complexes, with the synthesis of the mononuclear complex[3] $[Ru(bpy)_2(qH_2{\cdot}catH_4)](PF_6)_2$ and the symmetric dinuclear $[(Ru(bpy)_2)_2(qH_2{\cdot}qH_2)](PF_6)_4$ complex.[4] These species and several of their reduced forms, including a mixed valence quinone–semiquinonate form, were characterized electrochemically and spectroscopically.

These studies and previous work in the literature[7] dealing with dinuclear ruthenium complexes of the ligands 3,3′,4,4′-tetrahydroxobiphenyl, 3,3″,4,4″-tetrahydroxo-*p*-terphenyl, and 1,4,5,8-tetrahydroxonaphthalene, and related ligands, involve

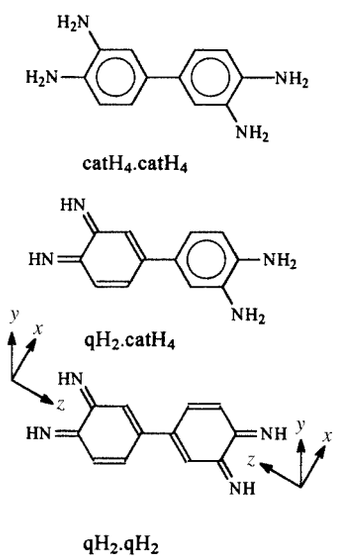

Fig. 1 Sketches of the bridging ligands showing the coordinate frame of reference used. The planar ligand lies in the *xz* plane. Note the orientations of the axis vectors as a guide to the signs used in the wavefunctions. The centrosymmetric conformer of $(qH_2{\cdot}qH_2)$ of C_{2h} symmetry is shown. By rotating one ring 180° about the central linking C–C bond, one obtains the planar acentric C_{2v} conformer.

† *Supplementary data available*: pictures of the molecular orbitals of the various species and xyz files for all of the species. For direct electronic access see http://www.rsc.org/suppdata/dt/1999/2653/, otherwise available from http://www.chem.yorku.ca/profs/lever/blever.htm, BLDSC (No. SUP 57592, 18 pp.) or the RSC Library. See Instructions for Authors, 1999, Issue 1 (http://www.rsc.org/dalton).

‡ *Current address*: Department of Chemistry, University of Waterloo, Waterloo, Ontario, Canada, N2L 3G1.

§ *Current address*: Depto. de Química Orgânica e Inorgânica, Centro de Ciências, Universidade Federal do Ceará, Campus do Pici, Fortaleza, Ce., Cx. Postal 12200, Brasil.

very strongly coupled metal–ligand interactions. Such species may form the basis for the synthesis of molecular electronic devices.

In this contribution, the ($catH_4$·$catH_4$) ligand was used to synthesize the dinuclear ruthenium complexes $[(Ru(NH_3)_4)_2(catH_4{\cdot}catH_4)](PF_6)_4$ and $[Ru(NH_3)_4(catH_4{\cdot}catH_4)Ru(bpy)_2](PF_6)_4$ referred to as the symmetric and asymmetric species respectively. Controlled oxidation of the ($catH_4$·$catH_4$) species gives rise to a series of complexes with a range of oxidation states whose nature is the subject of this contribution. In addition to the fully oxidized ligand species, $[(Ru(NH_3)_4)_2(qH_2{\cdot}qH_2)]^{4+}$ and $[Ru(NH_3)_4(qH_2{\cdot}qH_2)Ru(bpy)_2]^{4+}$ we demonstrate the existence of complexes containing the mixed valence (qH_2·$catH_4$) bridge as well as mixed valence Ru(III)/Ru(II) species. The complexes are characterized by a wide range of techniques including NMR, EPR, UV–VIS spectroscopy, electrospray ionization mass spectrometry (ESI-MS) and electrochemistry.

ZINDO/1 geometry optimizations and ZINDO/S spectroscopic calculations[8] were also performed on this series of complexes. Good agreement was achieved, with closed shell species, between observed and ZINDO/S predicted electronic spectra and the electronic structure of these complexes was deduced therefrom.

Extensive mixing between ruthenium d_π orbitals and ligand π and π* orbitals is observed when either or both ends of the bridging ligand are in the qH_2 oxidation state. The extent of mixing is discussed in terms of the net oxidation state of the species. These studies extend the recent contributions[9,10] on ruthenium pyridine, bipyridine and pyrazine coupling adding to our knowledge of the more complex dinuclear species.[11] They further confirm the notion that electron rich Ru(II) fragments such as the $[Ru(NH_3)_4]^{2+}$ moiety can couple extremely strongly to organic fragments such as benzoquinonediimine through both the π and π* frameworks.[1–4]

Experimental

All chemical products used were reagent quality or better and were used without any further purification, unless otherwise stated. The water was doubly distilled, the second time from potassium permanganate, and passed through Barnstead activated charcoal and ion-exchange filters. All other solvents were distilled and dried following literature methods.[12]

Physical measurements

Electronic spectra were recorded on a Cary model 2400 spectrophotometer, or on a Hewlett Packard 8452A diode array instrument. Electrochemical measurements were recorded using Princeton Applied Research Corp. models 173, 174 and 179 instruments, or a Pine Instruments RDE-3 potentiostat. Results were obtained using either CH_3CN with 0.15 M tetrabutylammonium hexafluorophosphate ($TBAPF_6$) or phosphate buffer solutions, solutions typically contained 1×10^{-3} M of the complex. A platinum disk, or a glassy carbon disk served as the working electrode, a platinum wire as counter electrode, and an SCE, or AgCl/Ag coated wire was used as the reference electrode. In cases where AgCl/Ag was used as the reference electrode, ferrocene was added as an internal standard, and the potentials are reported *vs.* SCE assuming a ferrocenium–ferrocene potential of 0.425 V *vs.* SCE in CH_3CN.[13]

C, H and N microanalyses were performed by the Canadian Microanalytical Service, Vancouver, British Columbia, Canada, or the Laboratórios de Microanálise da Universidade de São Paulo - Sp - Brasil. Nuclear magnetic resonance (NMR) spectra were recorded with a Bruker AM300 NMR spectrometer. Spectra were recorded with acetone-d_6 as the solvent and tetramethylsilane (TMS) as standard.

The EPR spectra were recorded in a Bruker spectrometer model ESP300e and a microwave bridge model ER 041 XK (X band), coupled to a standard cavity model 941ST380, in a temperature range of 110 ± 5 K.

Table 1 Key bond distances (pm) of optimized structures

Species[a]	C=NH[b]	Ru–NH(bridge)[c]	Ru–NH_3[d]	Ru–N(bpy)
asymcc		207(am), 209(bpy)	216(ax), 214(eq)	204
asymqc	133	203(q), 209(cat)	216(ax), 214(eq)	204
asymqq	133	203(am), 204(bpy)	216(ax), 214(eq)	203
symcc		207	216(ax), 214(eq)	
symqc	133	203(q), 207(cat)	216(ax), 214(eq)	
symqq	133	203	216(ax), 214(eq)	

[a] Asymmetric and symmetric species: cc = $catH_4$·$catH_4$, qc = qH_2·$catH_4$, qq = qH_2·qH_2. [b] Bridge imine bond length. [c] Average Ru–N (bridge) bond length, am = tetrammine terminus, bpy = bipyridine terminus, q = qH_2 terminus, cat = $catH_4$ terminus. [d] ax = Axial, eq = equatorial, these distances were restrained in the optimization. See ESI for complete structural information as xyz files which may be directly viewed using CHIME.

INDO/1 and INDO/S calculations used the ZINDO method and the Hyperchem software package (v5.1, Hypercube, Florida, USA). Data were processed on a Silicon Graphics Personal Iris Indigo R4000 or a Pentium 120 MHz Intel computer. Structures of all complexes were obtained by using the modified INDO/1 semiempirical method (ZINDO/1) in the Hyperchem program. The recommended value[8b] of the 'resonance' integral parameter for Ru, β(4d) = −26.5 eV overestimates the Ru–N bond strength and produces rather short Ru–N distances. Better agreement with X-ray structural data for these complexes was obtained by using a value[14] of β(4d) = −20 eV. All other parameters used in ZINDO/1 were the default parameters in the Hyperchem program. Convergence was assumed when the gradient was lower than 30 cal mol^{-1} $Å^{-1}$. All bond distances and angles in the optimised structures lay within accepted norms for these types of molecule, see Table 1. Full details of the optimised structures are available as electronic supplementary information (ESI) as xyz files which may be directly viewed using CHIME.

The ZINDO/S programme used the ruthenium bases provided by Krogh-Jespersen *et al.*[15] Electronic spectra were calculated with single excitation configuration interaction (CIS).[16] The number of configurations used was 20 occupied × 20 unoccupied orbitals. Reasonable convergence of calculated transition energies in the visible region was achieved, and increasing the number of configurations had an insignificant effect on the predicted visible region absorption energies. The overlap weighting factors σ–σ and π–π were set at 1.267 and 0.585, respectively. Small variations in these parameter values had no substantive effect on the calculations. Oscillator strengths were calculated in the dipole length approximation including the one-centre sp and pd atomic terms.

Electrospray ionization mass spectrometry (ESI-MS)[17,18]

Solution electrospray ionization mass spectrometry (ESI-MS) in analytical grade CH_3COCH_3 or CH_3CN was performed using a Sciex TAGA MS/MS spectrometer, at 2.8 kV applied voltage on the electrospray probe. For the ESI-MS data, mass and intensities were compared to those calculated using the Isopro 3.0 version MS/MS software for PC.

Synthesis

All syntheses were performed under an inert atmosphere, unless otherwise noted. The starting complexes $[Ru(NH_3)_5Cl]Cl_2$, $Ru(bpy)_2Cl_2{\cdot}2H_2O$ and *cis*-$[Ru(NH_3)_4(H_2O)_2](CF_3SO_3)_3$ were prepared following literature procedures.[19,20] The ligand 3,3′,4,4′-tetraminobiphenyl tetrahydrochloride dihydrate and the complex $RuCl_3{\cdot}3H_2O$ were purchased from Aldrich.

Table 2 NMR results of symmetric and asymmetric complexes (s and m represent singlet or multiplet). All spectra were recorded in acetone-d_6 unless otherwise noted

Complex	δ (ppm)	Assignment
$[(Ru(NH_3)_4)_2(catH_4{\cdot}catH_4)]^{4+}$	2.48 (s)	Axial NH_3
	2.68 (s)	Equatorial NH_3
	5.81 (s)	$(catH_4{\cdot}catH_4)$ amino
	7.52 (m), 7.69 (s)	$(catH_4{\cdot}catH_4)$ ring protons
$[Ru(NH_3)_4)_2(qH_2{\cdot}qH_2)]^{4+}$	2.48 (s)	Axial NH_3
	4.51 (s), 4.65 (s)	Equatorial NH_3
	7.38 (d), 7.57 (d), 7.89 (s)	$(qH_2{\cdot}qH_2)$ ring protons
	12.22 (s), 12.26 (s)	Imine protons
$[Ru(bpy)_2(catH_4{\cdot}catH_4)Ru(NH_3)_4]^{4+}$	2.48 (s)	Axial NH_3
	4.63 (s), 4.54 (s)	Equatorial NH_3
	6.25 (m), 6.75 (m)	$(catH_4{\cdot}catH_4)$ amino
	7.1–9.2	bpy and $(catH_4{\cdot}catH_4)$ ring protons
$[Ru(bpy)_2(qH_2{\cdot}qH_2)Ru(NH_3)_4]^{4+}$	2.51 (s)	Axial NH_3
	4.48 (s), 4.77 (s)	Equatorial NH_3
	7.25–8.85	$(qH_2{\cdot}qH_2)$ and bpy protons
	13.0 (s), 12.9 (s), 12.4 (s), 12.25 (s)	Imine protons
$[(Ru(bpy)_2)_2(qH_2{\cdot}qH_2)]^{4+}$ [a]	7.27–8.50	$(qH_2{\cdot}qH_2)$ and bpy protons
	12.08 (s), 11.98 (s)	Imine protons
$[Ru(bpy)_2(dadib)]^{2+}$ [b]	3.84 (s), 4.18 (s)	dadib amino protons
	6.70–8.48	dadib and bpy protons
	11.32 (s), 11.78 (s)	Imine protons
$[Ru(NH_3)_4(bqdi)]^{2+}$ [c]	2.30 (s)	Axial NH_3
	4.60 (s)	Equatorial NH_3
	6.85 (d), 7.45 (d)	bqdi ring protons
	12.25 (s)	Imine protons

[a] Recorded in DMSO-d_6. [b] Recorded in CD_3CN, dadib = 3,4-diamino-3′,4′-diimino-3′,4′-dihydrobiphenyl. [c] bqdi = *o*-benzoquinonediimine.

(a) $[(Ru(NH_3)_4)_2(catH_4{\cdot}catH_4)](PF_6)_4$. *cis*-$[Ru(NH_3)_4(H_2O)_2](CF_3SO_3)_3$ (0.137 g, 0.21 mmol) was dissolved in an aqueous solution (2 mL), pH = 2.0 (CF_3CO_2H used to adjust the pH) in the presence of zinc amalgam (3.0 g), and the solution was bubbled with argon. After 30 min the Ru(III) complex had been reduced to Ru(II) and was transferred to a separate flask. An aqueous deoxygenated solution (3 mL) containing 3,3′,4,4′-tetraminobiphenyl tetrahydrochloride dihydrate (0.042 g, 0.105 mmol) was added to the solution containing the ruthenium(II) tetrammine species. The reaction mixture was stirred for 2 h, and then with the addition of 1 mL of a saturated aqueous solution of NH_4PF_6, a yellow microcrystalline solid precipitated. The yellow solid was collected by filtration under an inert atmosphere, washed with deoxygenated ethanol and diethyl ether, dried and stored under vacuum in a desiccator. Yield 70% (Calc. for $C_{12}H_{34}F_{24}N_{12}P_5Ru_2$: C, 12.77; H, 3.04; N, 14.89. Found: C, 12.47; H, 3.19; N, 13.08%). Difficulty was experienced in obtaining a satisfactory nitrogen analysis.

(b) $[Ru(NH_3)_4(catH_4{\cdot}catH_4)Ru(bpy)_2](PF_6)_4$. The complex was prepared by adding $Ru(bpy)_2Cl{\cdot}2H_2O$ (0.1 g, 0.19 mmol) in deoxygenated water, 10 ml, pH = 2.0, containing 3,3′,4,4′-tetraminobiphenyl tetrahydrochloride dihydrate (0.075 g, 0.19 mmol). The mixture was heated at 40 °C for 24 h, during which time the initial purple–black suspension became an orange solution. At this point, the mononuclear complex $[Ru(bpy)_2(catH_4{\cdot}catH_4)]^{2+}$ had been formed in solution. This was then allowed to cool to room temperature. *cis*-$[Ru(NH_3)_4(H_2O)_2](CF_3SO_3)_3$ (0.12 g, 0.19 mmol) was dissolved in deoxygenated water (2 mL), pH = 2.0, in the presence of zinc amalgam (3.0 g). After 30 min, during which time the Ru(III) complex was reduced to Ru(II), the solution was transferred into the flask which contained the $[Ru(bpy)_2(catH_4{\cdot}catH_4)]^{2+}$ complex. This mixture was stirred for 4 h, at room temperature. Then, with the addition of 1 mL of a saturated aqueous solution of NH_4PF_6, an orange solid precipitated from the solution. The solid was collected by filtration, under an inert atmosphere, and washed with degassed ethanol and diethyl ether. The product was dried and kept under vacuum in a desiccator. Yield 68% (Calc. for $C_{32}H_{38}F_{24}N_{12}P_4Ru_2$: C, 27.99; H, 2.79; N, 12.24. Found: C, 28.15; H, 3.00; N, 11.43%). Difficulty was experienced in obtaining a satisfactory nitrogen analysis.

The oxidation of the fully reduced $(catH_4{\cdot}catH_4)$ solids by the addition of[1–5] NH_3 and O_2 yielded solutions of the symmetric and asymmetric species in the Ru(II)$(qH_2{\cdot}qH_2)$Ru(II) oxidation state as indicated by their electronic spectra. However the *solids* isolated by this route were EPR active, giving a Ru(III) signal. In solution these oxidized complexes are EPR silent. Evidently the solid state favours formation of a Ru(III) species electronic isomer which is not observed in the solution oxidation process under similar conditions (NH_3,O_2). The reactivity and characterization of these oxidized solids are the subject of a future contribution.[21]

Results

NMR and ESI-MS spectroscopy

Details of the NMR data for these complexes and related species are listed in Table 2.

$[(Ru(NH_3)_4)_2(catH_4{\cdot}catH_4)]^{4+}$. In this symmetric, reduced complex, the structure is confirmed by the two sets of resonances for the equivalent pairs of axial and equatorial amine protons, and the signals, at δ 7.52 and 7.69 that are assigned to the protons of the $(catH_4{\cdot}catH_4)$ ligand. The NMR spectra of axially and equatorially oriented NH_3–Ru protons have been extensively discussed.[11b,22]

$[(Ru(NH_3)_4)_2(qH_2{\cdot}qH_2)]^{4+}$. The NMR spectrum of this symmetric oxidized species in consistent with the proposed structure. The position of the axial NH_3 protons is unchanged compared to the fully reduced complex while the equatorial NH_3 protons are shifted downfield. These protons are deshielded by the relatively electron deficient (qH_2) fragment and appear as two signals because the two imine functions are inequivalent. The existence of a singlet and two doublets in the aromatic region accounts for the protons of the $(qH_2{\cdot}qH_2)$ ligand. The imino protons appear as two singlet resonances located downfield at δ 12.22 and 12.26 which is consistent with the NMR spectra of related complexes.[1–5]

The corrected ESI-MS spectrum of this symmetric (qH_2·qH_2) species in CH_3CN shows the presence of several quadruply charged species. The parent ion was observed at *m/z* 138.25 as an envelope of peaks associated with the ruthenium isotopes. In addition, peaks were observed at *m/z* 148.5, 158.75, 169 and 179.25 corresponding to the cluster formation of the symmetric species with one, two, three and four CH_3CN molecules respectively. The isotopic distribution of these species was in good agreement with the calculated composition. Such cluster assemblies are well known in ESI-MS spectroscopy.[17] Other relevant species that could be identified are at *m/z* 164.75 and 175 corresponding to the loss of one NH_3 group from three and four CH_3CN clusters respectively.

$[Ru(NH_3)_4(catH_4{\cdot}catH_4)Ru(bpy)_2)]^{4+}$. The NMR spectrum of this asymmetric ion is complicated by its low symmetry. There are a large number of peaks in the aromatic region which correspond to the bpy[23] protons and the protons of the ($catH_4$·$catH_4$) ligand. The amino groups of the ($catH_4$·$catH_4$) ligand appear as two multiple signals. All four amino groups are shifted downfield, compared to the symmetric dinuclear complex $[(Ru(NH_3)_4)_2(catH_4{\cdot}catH_4)]^{4+}$. The amino groups appear as multiple signals for two reasons. In the asymmetric complex the four amino groups are inequivalent and there is also a chiral $[Ru(bpy)_2]^{2+}$ centre in this complex whose presence makes the protons of the amino groups diastereotopic.[24] These factors put each proton of each amino group into a magnetically different environment, which produces coupling between the protons on each amino group. Considering the appearance of the NMR spectrum of the $[Ru(bpy)_2(dadib)]^{2+}$ complex, listed in Table 2, which shows two different amino signals, it seems likely that the 3- and 3′-amino groups will be similar and the 4- and 4′-amino groups will be similar.

The axial ammines of the $[Ru(NH_3)_4]^{2+}$ fragment are in almost the same location as they are in the symmetric complex, but the equatorial ammines are shifted downfield relative to the symmetric complex and appear as two signals. The cause of this shift may be the $[Ru(bpy)_2]^{2+}$ fragment which acts as an electron-withdrawing group compared to $[Ru(NH_3)_4]^{2+}$. The inequivalent amino groups will shield the amine ligands to slightly different degrees producing two signals.

$[Ru(NH_3)_4(qH_2{\cdot}qH_2)Ru(bpy)_2]^{4+}$. The NMR spectrum of this asymmetric oxidized species is consistent with the proposed structure. The axial NH_3 groups are essential in the same position as they are in every complex in this series, while the equatorial ammine groups are shifted downfield, relative to the ($catH_4$·$catH_4$) complex, as they are in the symmetric species. The protons of the bpy and phenyl rings of the (qH_2·qH_2) ligand appear as multiplets in the aromatic region. The imino protons on the Ru–bpy fragment and the Ru–NH_3 fragment each appear as two singlet resonances with a 1 : 1 intensity ratio.

The corrected ESI-MS spectrum of this asymmetric (qH_2·qH_2) species in acetone shows the formation of several doubly charged species. The predominant species which were observed at *m/z* 396.5, 388, 379.5, 371, 363.5 correspond to the 2+ charged species and those with the loss of one, two, three and four NH_3 groups respectively. The isotopic distribution observed for these species is in good agreement with the calculated composition. Formation of lower charged complexes in the ESI-MS has previously been observed[18] to occur *via* proton abstraction by ions such as F^-, which is a fragment ion of PF_6^-. We expect a similar process to occur in our case, as the protons on the ammine groups are relatively acidic and thus could react with F^- from the PF_6^- counter ion forming HF.

Redox chemistry

(a) Electrochemistry. The typical electrochemical behaviour for complexes of this type of ligand[1–5] in the quinonediimine oxidation state, when investigated using cyclic voltammetry shows two reversible one-electron reduction processes at the ligand to form first the semiquinonediimine, and then the deprotonated diamide (only one proton per amino group, ($catH_2$) as opposed to two) oxidation states. The metal may also be oxidized from Ru(II) to Ru(III).

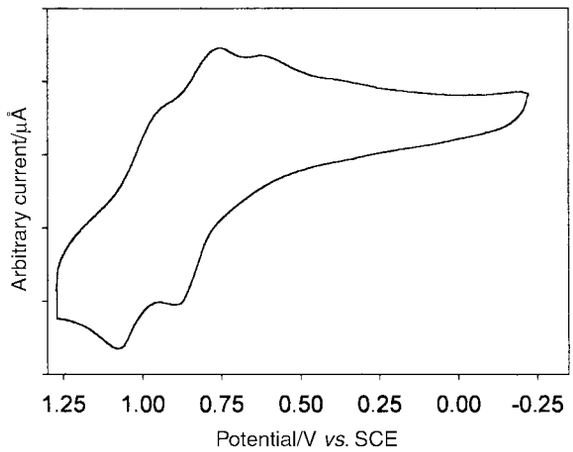

Fig. 2 Cyclic voltammogram of $[(Ru(NH_3)_4)_2(qH_2{\cdot}qH_2)]^{4+}$ in acetonitrile solution (0.15 M $TBAPF_6$). Scan rate 100 mV s^{-1}.

In the case of symmetric and asymmetric ruthenium complexes of the ($catH_4$·$catH_4$) ligand having two *o*-phenylenediamine ligands bonded together, no well defined ligand centred redox processes were observed in the cyclic voltammetry in organic solvents. All processes appeared to be irreversible in the several different solvents explored.

However oxidation of the metal centres in these complexes can be seen in the CV experiments. Fig. 2 shows the oxidation of the oxidized symmetric product; $[(Ru(NH_3)_4)_2(qH_2{\cdot}qH_2)]^{4+}$ in acetonitrile. This complex has one process at 0.86 V (*vs.* SCE), which corresponds to the oxidation of one ruthenium atom from Ru(II) to Ru(III), to generate the mixed valence $[(NH_3)_4Ru^{II}(qH_2{\cdot}qH_2)Ru^{III}(NH_3)_4]^{5+}$ (abbreviated as [II,III-(qH_2·qH_2)] species. A second oxidation process occurs at 1.04 V (*vs.* SCE), corresponding to the oxidation of the second ruthenium atom to generate the [III,III-(qH_2·qH_2)]. The small signal at 0.65 V likely represents the reduction of a decomposition product, as this peak is not observed until potentials more positive of the first oxidation are reached.

The $\Delta E'$ between the [II,III-(qH_2·qH_2)] and [III-III(qH_2·qH_2)] redox processes, is 0.18 V which is 60 mV greater than the corresponding processes in the symmetric bipyridine species[4] $[(Ru(bpy)_2)_2(qH_2{\cdot}qH_2)]^{4+}$. The increase in $\Delta E'$ value reflects greater electron delocalization between the two Ru(II) centres due to replacing the bpy ligands with the more basic NH_3 ligands. This value of $\Delta E'$ is comparable to that observed for the 2,2′-bipyrimidine bridged bis $[Ru(NH_3)_4]^{2+}$ dinuclear complex (0.19 V)[25] and is much larger than the $\Delta E'$ values observed for many of the complexes of monodentate bridging ligands ($\Delta E'$ = 50–80 mV), with the exception of pyrazine ($\Delta E'$ = 0.39 V).[26]

The value of $\Delta E'$ allows one to calculate the comproportionation constant, K_c for the following comproportionation reaction [eqn. (1)].

$$[II,II\text{-}(qH_2{\cdot}qH_2)]^{4+} + [III,III\text{-}(qH_2{\cdot}qH_2)]^{6+} \rightleftharpoons 2\,[II,III\text{-}(qH_2{\cdot}qH_2)]^{5+} \quad (1)$$

K_c has a value of 1.1×10^3 which is approximately 10 times the K_c value of 100 calculated for $[(Ru(bpy)_2)_2(qH_2{\cdot}qH_2)]^{4+}$ based on the reported $\Delta E'$.[5]

The asymmetric product $[Ru(NH_3)_4(qH_2{\cdot}qH_2)Ru(bpy)_2]^{4+}$ has its first oxidation at 0.87 V (*vs.* SCE) which is assigned as oxidation of the ruthenium tetrammine fragment from Ru(II) to

Ru(III), to generate the $[Ru^{III}(NH_3)_4(qH_2{\cdot}qH_2)Ru^{II}(bpy)_2]^{5+}$ mixed valence species. The second oxidation occurs at 1.42 V (*vs.* SCE) and corresponds to the oxidation of the $[Ru(bpy)_2]$ fragment from Ru(II) to Ru(III). There are some small bumps in the region of 1.0 V which are likely due to decomposition products of the mixed valence species. The splitting between the formation of the $[Ru^{III}(NH_3)_4(qH_2{\cdot}qH_2)Ru^{II}(bpy)_2]^{5+}$ species and the $[Ru^{III}(NH_3)_4(qH_2{\cdot}qH_2)Ru^{III}(bpy)_2]^{6+}$ species is 0.55 V, approximately 130 mV less than in the asymmetric dinuclear complex of bipyrimidine.[25] For the asymmetric complex the evaluation of K_c based upon $\Delta E'$ does not have the same meaning as it does for a symmetric dinuclear complex but also reflects the significant difference in the local environment of the two metal centres. This is undoubtedly a valence trapped mixed valence species. The complex, in the frozen solution state, exhibits a broad poorly resolved EPR signal close to $g = 2$. Some additional data for these species are presented below.

(b) Chemical oxidation/spectroelectrochemistry. As indicated, these species potentially have five oxidation states accessible to the bridging ligand (two pairs of $catH_4 \longrightarrow sqH_2 \longrightarrow qH_2$), two oxidation states readily accessible to the metal centre (Ru(II)/Ru(III)) and in the case of the asymmetric species, additional oxidation states associated with reduction of the bipyridine fragments. We are concerned with characterizing as many of these oxidation states as possible and assessing their electronic structures. This can in principle be achieved by controlled potential oxidations and reductions, and by chemical oxidation or reduction. Both of these techniques have been employed and yield similar data. The chemical oxidations can be controlled readily by adding specific equivalents of oxidizing agent to the $Ru^{II}(catH_4{\cdot}catH_4)Ru^{II}$ species, dissolved in 0.1 M phosphoric acid, and these data will be described first. The individual species can be defined through their electronic spectra. In both the symmetric and asymmetric species the initial starting material can be described by $Ru^{II}(catH_4{\cdot}catH_4)Ru^{II}$ and four-electron oxidation will yield the species $Ru^{II}(qH_2{\cdot}qH_2)Ru^{II}$. In principle one might expect to see the successive oxidation of the bridging ligand as one proceeds from $Ru^{II}(catH_4{\cdot}catH_4)Ru^{II}$ with one, two, three and four equivalents of oxidizing agent.

The spectra obtained upon successive step-wise oxidation of the symmetric and asymmetric ($catH_4{\cdot}catH_4$) species are shown in Fig. 3 and 4. These spectra can be demonstrated to be composites of the spectrum of the starting material $[Ru^{II}(catH_4{\cdot}catH_4)Ru^{II}]$, the spectrum of the final product, $[Ru^{II}(qH_2{\cdot}qH_2)Ru^{II}]$ and the spectrum of only one intermediate species which we demonstrate below is generically $[Ru^{II}(qH_2{\cdot}catH_4)Ru^{II}]$. No evidence was ever found for a semiquinonate species (as identifiable through its electronic spectrum), nor were any bands associated with ligand to Ru(III) LMCT observed (up to four-electron oxidation per dinuclear molecule).

The Ru $\longrightarrow$ sq transition usually occurs as an intense band at very low energies, for example in the $[(Ru(bpy)_2)_2(sq,sq)]^{2+}$ complex the Ru $\longrightarrow$ sq transition is at 9260 cm^{-1}, while in the $[(Ru(bpy)_2)_2(q,sq)]^{3+}$ complex it is at 8160 cm^{-1}.[4] The Ru(III) spectra of related species,[1] have a narrow intense transition at *ca.* 24000 cm^{-1}. No evidence of either of these transitions was observed in the first four oxidation steps from $[Ru^{II}(catH_4{\cdot}catH_4)Ru^{II}]$. This is true irrespective of whether the system was oxidized with ceric ion [Ce(IV)] or $S_2O_8^{2-}$. The intermediate species can then only be $[Ru^{II}(qH_2{\cdot}catH_4)Ru^{II}]$ and we demonstrate below that its formation and electronic spectrum are consistent with this formulation.

There are two geometric isomers of the asymmetric intermediate $[Ru^{II}(NH_3)_4(qH_2{\cdot}catH_4)Ru^{II}(bpy)_2]^{4+}$ and $[Ru^{II}(NH_3)_4(catH_4{\cdot}qH_2)Ru^{II}(bpy)_2]^{4+}$. Oxidation of the $Ru^{II}(catH_4..)$ fragment to $Ru^{II}(qH_2..)$ proceeds *via* formation of a $Ru^{III}(catH_4..)$ intermediate (see detail in next section below). Previous literature experience [1a,4a,27] reveals that the $Ru^{II}(NH_3)_4(catH_4..)$ fragment is very much easier to oxidize than the $Ru^{II}(bpy)_2(catH_4..)$ fragment and we conclude therefore that the isomer generated is the former of the two cited above. Moreover a ZINDO/1 derivation of the heat of formation of the two isomers shows that the former is some 140 kcal mol^{-1} (in a total of −16840 kcal mol^{-1}) more stable than the latter.

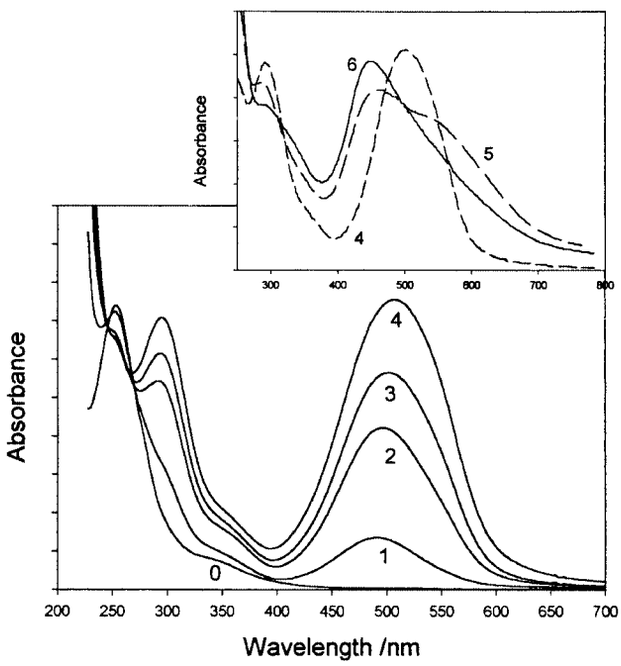

Fig. 3 Ceric titration of a 4.1×10^{-5} M solution of $[(Ru(NH_3)_4)_2(catH_4{\cdot}catH_4)](PF_6)_4$ in 0.1 M H_3PO_4 showing the addition of 0–4 equivalents of Ce(IV). Inset; data for 4–6 equivalents of Ce(IV) as designated.

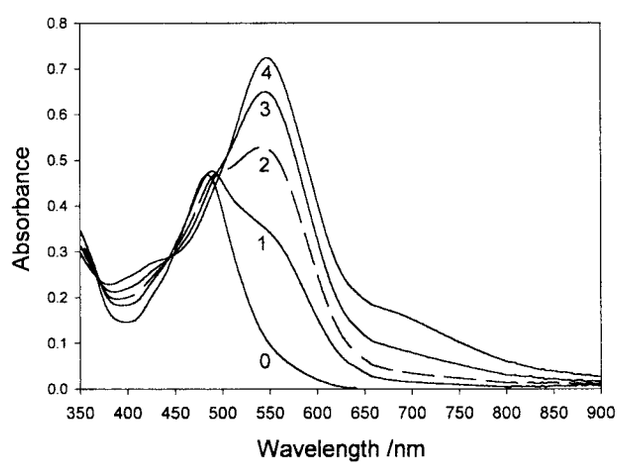

Fig. 4 Ceric titration of a 2.2×10^{-5} M solution of $[Ru(bpy)_2(catH_4{\cdot}catH_4)Ru(NH_3)_4](PF_6)_4$ in 0.1 M H_3PO_4 showing the addition of 0–4 equivalents of Ce(IV).

Thus after one equivalent of ceric ion (in 0.1 M H_3PO_4) has been added (one electron per dinuclear species) the solution contains 50% unchanged $Ru^{II}(catH_4{\cdot}catH_4)Ru^{II}$ and 50% $Ru^{II}(qH_2{\cdot}catH_4)Ru^{II}$, after two equivalents 100% $Ru^{II}(qH_2{\cdot}catH_4)Ru^{II}$, after three equivalents 50% each of $Ru^{II}(qH_2{\cdot}catH_4)Ru^{II}$ and $Ru^{II}(qH_2{\cdot}qH_2)Ru^{II}$ and finally 100% $Ru^{II}(qH_2{\cdot}qH_2)Ru^{II}$ after four equivalents have been added. The observed composite spectra of the one- and three-electron oxidized solutions can be simulated precisely by adding 50% of the spectrum of the fully reduced complex to 50% of the spectrum of the two-electron oxidized species and by adding 50% of the spectrum of the two-electron oxidized species to 50% of the spectrum of the four-electron oxidized species, respectively.

Further oxidation by ceric ion leads successively to the symmetric $[Ru^{III}(NH_3)_4(qH_2{\cdot}qH_2)Ru^{II}(NH_3)_4]^{5+}$ and $[Ru^{III}(NH_3)_4(qH_2{\cdot}qH_2)Ru^{III}(NH_3)_4]^{6+}$ species. With the asymmetric

species, one-electron oxidation to form $[Ru^{III}(NH_3)_4(qH_2{\cdot}qH_2)Ru^{II}(bpy)_2]^{5+}$ is feasible, but the Ce(IV) ion is incapable of oxidizing the $Ru^{II}(bpy)_2$ fragment to the Ru(III) product.

The spectroelectrochemical experiments were carried out beginning with the $[Ru^{II}(qH_2{\cdot}qH_2)Ru^{II}]^{4+}$ species and sequentially reducing back to $[Ru^{II}(catH_4{\cdot}catH_4)Ru^{II}]^{4+}$. The electronic spectra so obtained by controlled potential electrolysis (reduction) were the same as those obtained by appropriate chemical oxidation (Fig. 3 and 4) but obtained in the inverse sequence.

Fig. 3 (insert) shows the Ce(IV) ion oxidation of the symmetric species beginning with the $[Ru^{II}(qH_2{\cdot}qH_2)Ru^{II}]^{4+}$ species. The long wavelength tail on the $[Ru^{II}(qH_2{\cdot}qH_2)Ru^{III}]^{5+}$ species is very evident and is likely attributed to the expected intervalence band since this transition is not otherwise evident out to 1600 nm. This shoulder disappears in the spectrum of the [III,III-$(qH_2{\cdot}qH_2)$] species which, however, does show a long wavelength tail which must still encompass several transitions. Controlled potential oxidation of the $[Ru^{II}(qH_2{\cdot}qH_2)Ru^{III}]^{5+}$ species in acetonitrile (not shown) gave fairly similar spectra shifted somewhat because of the non-aqueous and aprotic solvent.[1d]

(c) Mechanism of oxidation. The absence of any semiquinonediimine species in the oxidation, chemical or electrochemical, of the $(catH_4{\cdot}catH_4)$ species, raises the question of the oxidation pathway which may be involved. The oxidation of a $(catH_4)$ to a (sqH_2) species involves both electron and proton loss and is generally electrochemically irreversible.[1] This is an example of oxidative dehydrogenation and the general mechanism *via* a higher oxidation state of the metal is very well documented.[28] If an acidic solution is used for the chemical oxidation, proton loss will be inhibited and the oxidation of a coordinated $-NH_2$ residue will lie at quite a high potential. The diamine fragment can be considered a substituted ammonia which would have a ligand electrochemical parameter value,[27] $E_L(L)$, near 0 V; thus oxidation of $[Ru^{II}(NH_3)_4(catH_4..)]$ to $[Ru^{III}(NH_3)_4(catH_4..)]^{3+}$ is expected to occur before oxidation of $(catH_4)$, with formation of $[Ru^{III}(catH_4{\cdot}catH_4)Ru^{II}]^{5+}$.

Evidence for this and a subsequent Ru(III) species has been obtained by EPR spectroscopy at low temperature. Thus a sample of the asymmetric $[Ru^{II}(NH_3)_4(catH_4{\cdot}catH_4)Ru^{II}(bpy)_2]^{4+}$ in 0.1 M phosphoric acid was frozen at liquid nitrogen temperature and contacted sequentially with 1–4 equivalents of ceric ion. The frozen solution was melted to allow for mixing and then it was refrozen. At liquid nitrogen temperature, EPR spectra consistent with the formation of a Ru(III) species[29] (and not of a free radical sqH_2 species) were observed upon addition of one ($g_\perp = 2.60$, $g_\parallel = 1.59$) or three ($g_\perp = 2.57$, $g_\parallel = 1.71$) Ce(IV) equivalents, but no signal with two or four equivalents. Upon warming to room temperature these signals disappeared.

The proposed sequence of steps involved in the oxidation is as follows.

(i) Addition of one equivalent of oxidant produces the following reaction [eqn. (2)].

$$[Ru^{II}(NH_3)_4(catH_4{\cdot}catH_4)Ru^{II}(bpy)_2]^{4+} \rightleftharpoons e^- + [Ru^{III}(NH_3)_4(catH_4{\cdot}catH_4)Ru^{II}(bpy)_2]^{5+} \quad (2)$$

(ii) When warmed towards room temperature the 5+ species disproportionates [eqn. (3)].

$$2\,[Ru^{III}(NH_3)_4(catH_4{\cdot}catH_4)Ru^{II}(bpy)_2]^{5+} \rightleftharpoons 2H^+ + [Ru^{II}(NH_3)_4(catH_4{\cdot}catH_4)Ru^{II}(bpy)_2]^{4+} + [Ru^{II}(NH_3)_4(qH_2{\cdot}catH_4)Ru^{II}(bpy)_2]^{4+} \quad (3)$$

(iii) After addition of a second equivalent of oxidant the solution is 100% $[Ru^{II}(NH_3)_4(qH_2{\cdot}catH_4)Ru^{II}(bpy)_2]^{4+}$.

(iv) The addition of a third equivalent of oxidant produces the following reaction [eqn. (4)].

$$[Ru^{II}(NH_3)_4(qH_2{\cdot}catH_4)Ru^{II}(bpy)_2]^{4+} \rightleftharpoons e^- + [Ru^{III}(NH_3)_4(qH_2{\cdot}catH_4)Ru^{II}(bpy)_2]^{5+} \quad (4)$$

(v) When warmed towards room temperature this species will disproportionate [eqn. (5)].

$$2\,[Ru^{III}(NH_3)_4(qH_2{\cdot}catH_4)Ru^{II}(bpy)_2]^{5+} \rightleftharpoons 2H^+ + [Ru^{II}(NH_3)_4(qH_2{\cdot}catH_4)Ru^{II}(bpy)_2]^{4+} + [Ru^{II}(NH_3)_4(qH_2{\cdot}qH_2)Ru^{II}(bpy)_2]^{4+} \quad (5)$$

(vi) The fourth equivalent of oxidant will convert the solution to 100% $[Ru^{II}(NH_3)_4(qH_2{\cdot}qH_2)Ru^{II}(bpy)_2]^{4+}$.

This proposed sequence of steps is consistent with the aforementioned observation of a Ru(III) EPR signal[29] at low temperature for the one- and three-electron oxidized species and no signal for the two- and four-electron oxidized species.

Similar experiments were performed on the symmetric species, but no EPR signals were seen for the addition of any number of equivalents of oxidant. This may be due to a more rapid disproportionation of the Ru(III) species.

ZINDO Calculations

ZINDO/1 calculations[8] were performed on this series of complexes in their different states of protonation and oxidation. The dihedral angle of the bridging ligand was free to rotate. The symmetric and asymmetric complexes optimized with dihedral angles of 69, 44 and 0° and 46, 35 and 4° respectively for the $(catH_4{\cdot}catH_4)$, $(qH_2{\cdot}catH_4)$ and $(qH_2{\cdot}qH_2)$ species. The size of the dihedral angle is governed by competition between the steric repulsion of the 2,6′- and 6,2′-hydrogen atoms and any electronic demands which might favour co-planarity. The $(qH_2{\cdot}qH_2)$ oxidation state can be expected to have a dihedral angle close to zero in order to maximise delocalization and ruthenium-bridge mixing. Delocalization and ruthenium-bridge mixing across the entire molecule are less likely in the $(catH_4{\cdot}catH_4)$ and $(qH_2{\cdot}catH_4)$ oxidation states, so steric repulsion will become the dominant factor and the dihedral angle will increase.

ZINDO/1 was used to derive heats of formation as a function of dihedral angle, primarily to assess how sensitive the heat is to the dihedral angle. In both the symmetric and asymmetric series of $(qH_2{\cdot}catH_4)$ and $(catH_4{\cdot}catH_4)$ the dependence is very flat with only a few kcal mol^{-1} separating the various conformers. We report below the optimized geometries but recognise that they may not be precisely accurate. The symmetric $(qH_2{\cdot}qH_2)$ shows the deepest well with the flat conformer, at −8846 kcal mol^{-1}, about 50 kcal mol^{-1} more stable than the 90° twisted conformer. The asymmetric $(qH_2{\cdot}qH_2)$ species shows similar behavior. Note however that there are two flat conformers depending upon the relative orientation of the two pairs of =NH groups (see Fig. 1). One conformer has a centrosymmetric bridge and the other does not. For the symmetric $(qH_2{\cdot}qH_2)$ species, these have C_{2h} and C_{2v} symmetry respectively. ZINDO/1 favours the centrosymmetric conformer in both the symmetric and asymmetric $(qH_2{\cdot}qH_2)$ species but only by a few kcal mol^{-1}. We assume henceforth that the centrosymmetric conformer is relevant for all the species under discussion.

The ZINDO/S single point calculations were carried out on the optimized structures even though in solution at room temperature, some rotation may occur about the central C–C bond.

(a) Free ligands. ZINDO/S calculations were performed on the free ligands using the optimized geometries that they have in the complexes. The flat $(qH_2{\cdot}qH_2)$ ligand has C_{2h} symmetry, the twisted $(qH_2{\cdot}catH_4)$ has C_1 symmetry and the twisted $(catH_4{\cdot}catH_4)$ has C_2 symmetry. The frontier orbitals of the $(qH_2{\cdot}qH_2)$ ligand include two pairs of filled π orbitals of b_g and a_u sym-

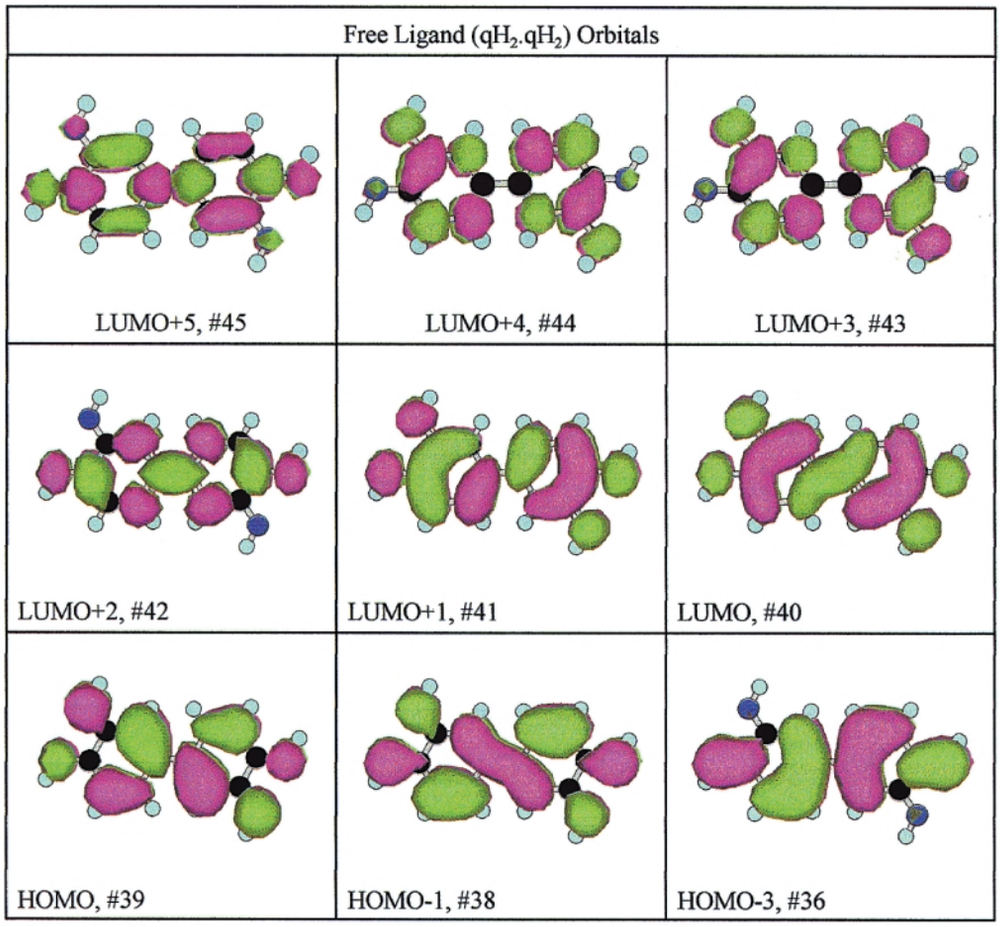

Fig. 5 A selection of ZINDO/S calculated frontier orbitals for the free (qH_2·qH_2) ligand of C_{2h} symmetry.

metry (#39,38,36,32) and three empty (π*) levels, a b_g orbital (LUMO + 1, #41) and a pair of a_u orbitals (LUMO #40, 42). Orbitals #40 and #41 are clearly the in and out of phase coupling of the π* levels of the two qH_2 fragments respectively (Fig. 5). Orbitals #36,42 and #43,44 have local density favoring opposite pairs of =NH groups.

The (qH_2·$catH_4$) ligand has frontier π and π* orbitals mostly spread over the entire bridge but with local symmetry at the qH_2 terminus very similar to that of the (qH_2·qH_2) bridge. The orbitals of the ($catH_4$·$catH_4$) ligand do not mix significantly with the metal d-orbitals.

(b) Complexes. It is convenient to define on each Ru center, a framework (Fig. 1) which would be appropriate for the local C_{2v} environment of the qH_2 ligand fragment. The bridge plane is then *xz*, and orbital d_{yz} is aligned to π-bond to a local qH_2 symmetric fragment, $d_{x^2-z^2}$ lies in the qH_2 plane and has σ-symmetry, d_{xy} has δ-symmetry with respect to qH_2; these then are filled with six electrons in the Ru(II) species. The empty d_{xz} and $d_{2y^2-x^2-z^2}$ point along Ru–N bond vectors and are σ*-antibonding.

Considering most simply the symmetric (qH_2·qH_2) species of C_{2h} symmetry, symmetry adapted orbitals comprising both Ru centres can be constructed from ($d_{xy} \pm d'_{xy}$), ($d_{yz} \pm d'_{yz}$) and ($d_{x^2-z^2} \pm d'_{x^2-z^2}$) where the primed and unprimed orbitals reside on different Ru centres. It is also possible to mix these orbitals on a given Ru atom, namely ($d_{xy} \pm d_{yz}$) so generating two orbitals of π-symmetry lying along the Ru–NH= (qH_2..) bond vectors. These too can linearly combine across the bridge to form symmetry adapted wavefunctions namely {($d_{xy} \pm d_{yz}$) ± ($d'_{xy} \mp d'_{yz}$)}. The π-orbitals described here transform exclusively as b_g if they are even with respect to inversion, and as a_u, if they are odd. They can then mix with the a_u and b_g π-orbitals of the bridging ligand to provide a mechanism for coupling the remote metals together. The ($d_{x^2-z^2} \pm d'_{x^2-z^2}$), combinations which lie in the bridge plane with σ-symmetry, transform as $a_g + b_u$. Some representative MO pictures are shown in Fig. 6. Others can be found as ESI.

In the low symmetry (C_1) asymmetric species coupling across the bridge can be assessed by the relative contributions of each Ru d orbital to the MOs. The resulting MO diagrams are shown in Fig. 6 while the fractional mixing in the frontier orbitals of these complexes can be seen pictorially in Fig. 7 (symmetric) and 8 (asymmetric), with energies displayed in Fig. 9 and 10. The asymmetric (qH_2·$catH_4$) appears a lot like a mononuclear $Ru(NH_3)_4(qH_2)$ species,[1a] with a substituent lowering its symmetry. Mixing, symmetry and energy data are collected in Table 3.

Orbital mixing

One important theme in past studies of these molecules is that of orbital mixing, and the extent of metal–ligand coupling. The extent of metal–ligand and metal–ligand–metal coupling can be probed as a function of the oxidation state of the bridging ligand. In the symmetric species, where the metal centres are chemically equivalent, *i.e.* $[(NH_3)_4Ru(catH_4{\cdot}catH_4)Ru(NH_3)_4]^{4+}$ and $[(NH_3)_4Ru(qH_2{\cdot}qH_2)Ru(NH_3)_4]^{4+}$, the difference in energy between the in- and out-of phase coupled pairs of equivalent d orbitals on each ruthenium is a measure of the extent of communication or coupling between the metal centres. In high symmetry such as D_{2h}, this splitting can be approximately related to the electronic matrix coupling element ($2H_{ab}$).[30] With $[(NH_3)_4Ru(qH_2{\cdot}qH_2)Ru(NH_3)_4]^{4+}$ the C_{2h} symmetry allows for some additional mixing of levels so that this energy difference can be used as a measure of communication but is not directly equal to $2H_{ab}$.

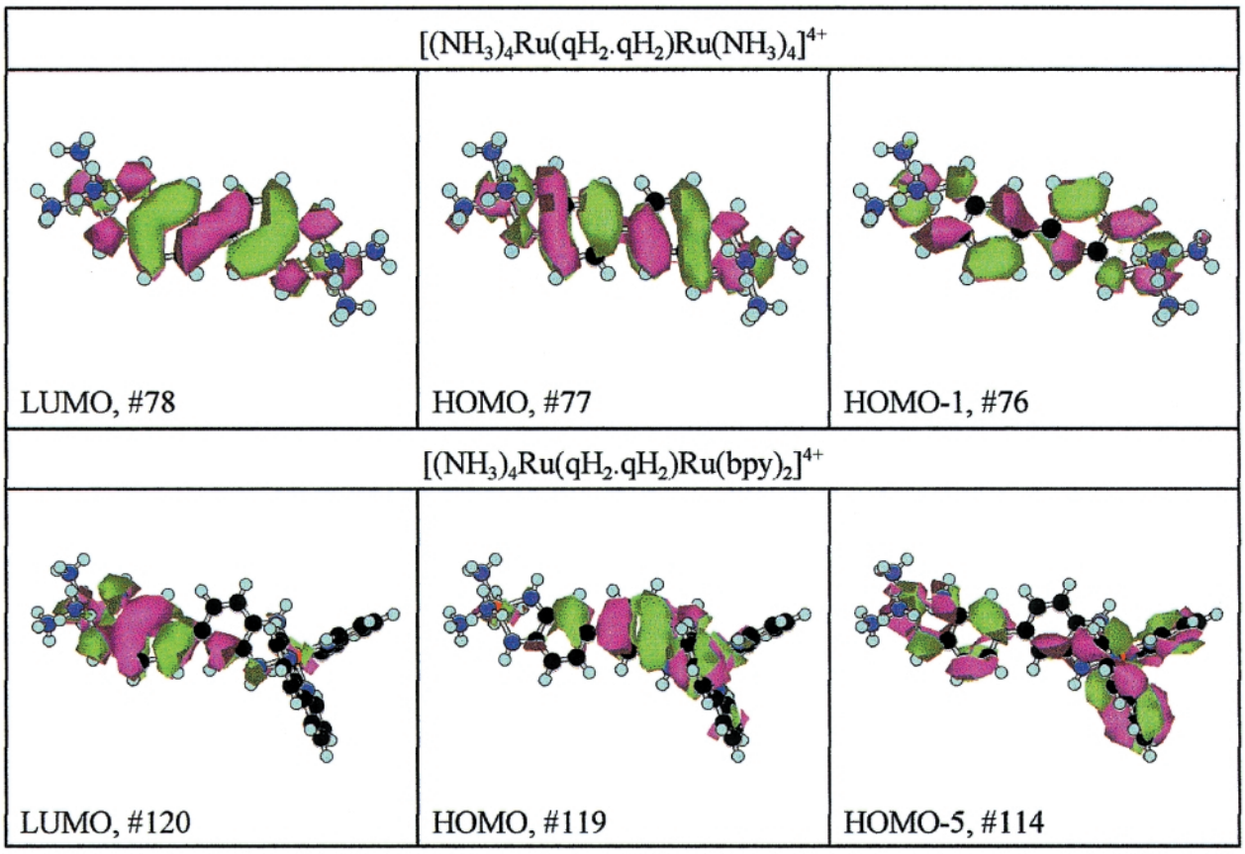

Fig. 6 A selection of ZINDO/S calculated frontier orbitals for (top) the symmetric (qH_2·qH_2) series of complexes and (bottom) the asymmetric (qH_2·qH_2) series of complexes. Additional examples can be found as electronic supplementary information.

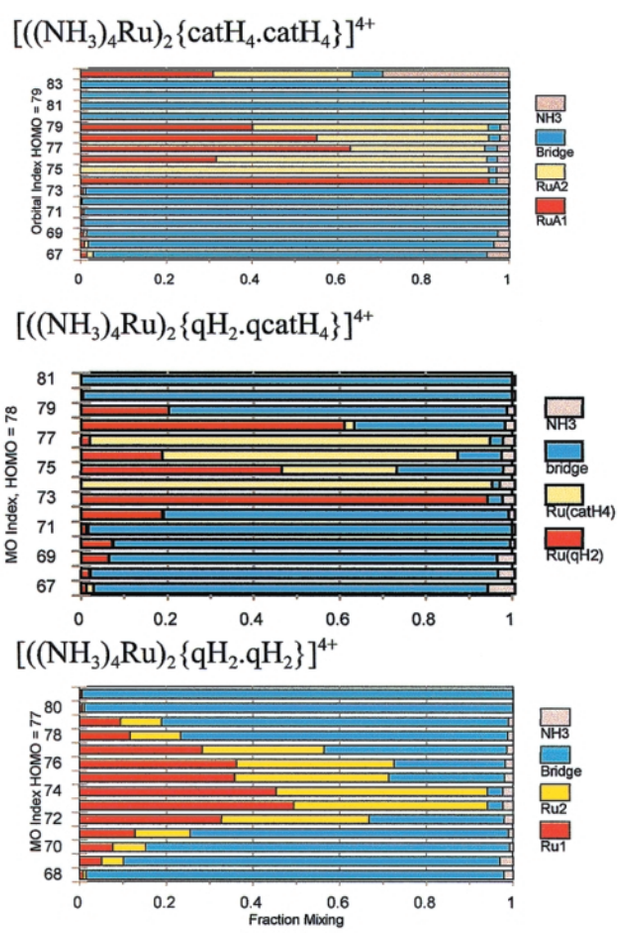

Fig. 7 ZINDO/S calculated fractional mixing for the symmetric series of complexes.

(a) ($catH_4$·$catH_4$) oxidation state. In this oxidation state the extent of metal–ligand mixing is very small. The *symmetric* complex has the six t_{2g} orbitals (HOMO–HOMO − 5, #79–#74) essentially unmixed (≤ 3%) with the bridging ligand (we use the octahedral t_{2g} label for convenience). These molecular orbitals are the in- and out-of-phase pairs of the atomic orbitals on each metal centre, combined by symmetry, rather than by any interaction, *i.e.* there is little if any communication between the orbitals on each ruthenium centre. The HOMO and HOMO − 1 (#79,78) are the σ-symmetry d(t_{2g}) orbitals. The energy separations between the in- and out-of-phase coupled pairs is less than 0.005 eV and this may just reflect slight asymmetry in the molecule following ZINDO optimization.

In the *asymmetric* species, the t_{2g} set of the $Ru(bpy)_2$ fragment (HOMO–HOMO − 2, #121–#119) are mixed (*ca.* 20%) with bpy π-orbitals, and unmixed (< 2%) with the bridging ligand orbitals. There are two bipyridine π-orbitals (#117,118) that lie, in energy, between the d-orbitals of the $[Ru(bpy)_2]$ fragment and the $[Ru(NH_3)_4]$ fragment.

The t_{2g} set of the $[Ru(NH_3)_4]$ fragment lies at deeper energy and two of these three orbitals are highly localized on ruthenium (*ca.* 90–100%). However there is a weak interaction between the d_{yz} combination and a bridge π-orbital (#113, 115) which does show some significant Ru d-bridge mixing probably owing to a good energy match. The splitting (interaction) energy is very small (*ca.* 0.09 eV).

(b) (qH_2·$catH_4$) oxidation state. In this oxidation state, significant metal–ligand mixing with the qH_2 end of the bridge is anticipated. The *symmetric* species optimizes with a large twist angle of 44° (Table 3). The HOMO (#78) is a mix of Ru d_π (qH_2) mixed with π-bridge, specifically an antibonding interaction, $(d_{yz} + d_{xy}) - \pi$. The HOMO − 1 (#77) is nearly pure d_σ-oriented orbital on the $catH_4$ end. HOMO − 2 and HOMO − 3 (#76,75) orbitals are in- and out-of-phase mixtures

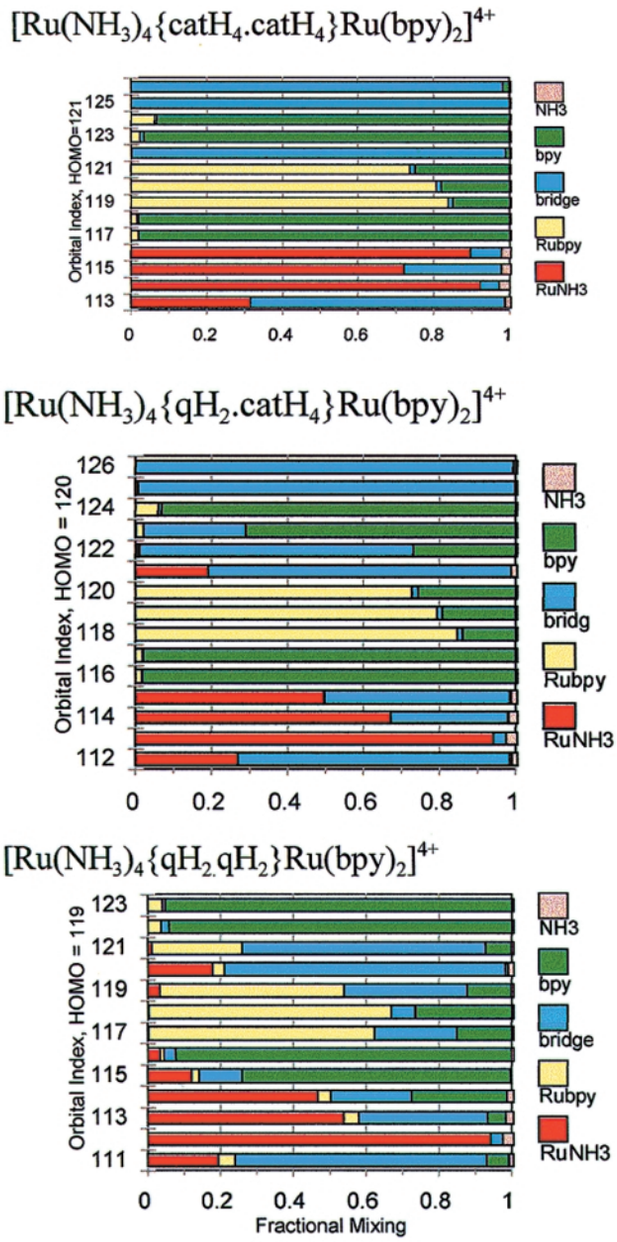

Fig. 8 ZINDO/S calculated fractional mixing for the asymmetric series of complexes.

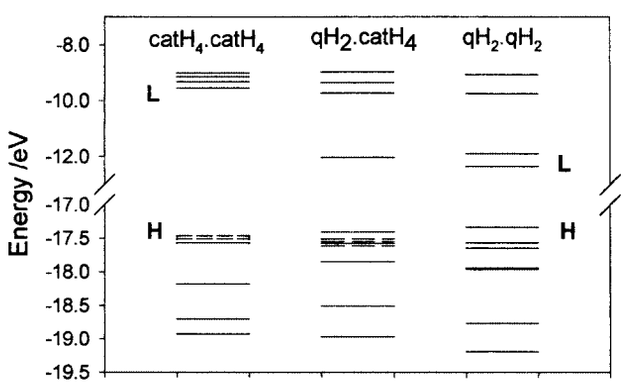

Fig. 9 Relative molecular orbital energies of the symmetric series as labelled. The HOMO is indicated by H and the LUMO by L. The $catH_4$ localized Ru $d(t_{2g})$ orbitals are displayed with hatched lines in the $catH_4$·$catH_4$ and qH_2·$catH_4$ species.

of d orbitals on both ends of the molecule with the bridging ligand. However these two orbitals are essentially degenerate and there is no significant coupling across the bridge.

The HOMO − 4, (#74) orbital is nearly pure d_{yz} orbital on

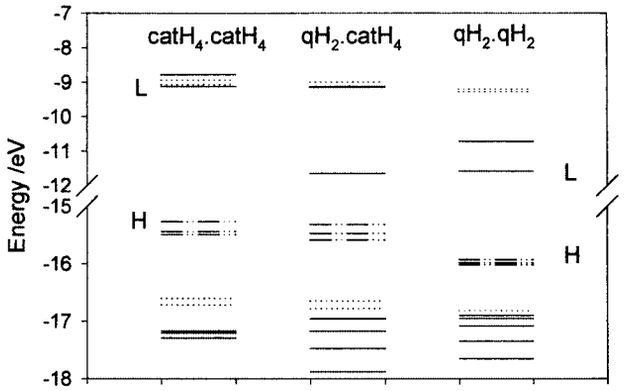

Fig. 10 Relative molecular orbital energies of the asymmetric series as labelled. The HOMO is indicated by H and the LUMO by L. In this case, the bipyridine localized orbitals are dotted, and the Ru $d(t_{2g})$ bpy localized orbitals by a hatched line. The solid lines indicate orbitals which are fairly extensively mixed as seen in Table 3.

the $catH_4$ end of the molecule, while HOMO − 5 (#73) is a fairly pure σ-oriented orbital on the qH_2 end (Table 3). By comparison with the asymmetric (qH_2·$catH_4$) species discussed below, it is surprising that the HOMO is localized on the qH_2 end of the molecule. This is seen to arise from a strong interaction between a bridge π-orbital coupling with (d_{yz} + d_{xy}) to provide the stabilized Ru–LL bonding combination HOMO − 6 (#72) and the destabilized Ru–LL antibonding combination HOMO (#78).

The *asymmetric* (qH_2·$catH_4$) species optimizes with an appreciable twist angle of *ca.* 35°. The t_{2g} set of the $Ru(bpy)_2$ fragment (which is bound to the ($catH_4$) end of the bridge) forms the HOMO, HOMO − 1 and HOMO − 2 (#120–#118) and is mixed with the bpy π* orbitals, but not mixed with the bridging ligand. Two bpy orbitals (#116,117) lie between these $Ru(bpy)_2$ d(t2g) orbitals and the $Ru(NH_3)_4$ $d(t_{2g})$ orbitals.

HOMO − 5, − 6 (#115,114) comprise d_{xy} − π and (d_{yz} − d_{xy}) − π respectively (albeit rather distorted by the low symmetry) while the σ–d orbital is HOMO − 7 (#113). The (d_{yz} + d_{xy}) orbital again mixes strongly with a localized qH_2 bridge π-orbital forming HOMO − 8 (#112) and HOMO − 5 (#115) which are Ru–LL bonding and antibonding respectively. This last orbital is only some 50% metal localized as a consequence of this extensive mixing.

The LUMO is an antibonding combination of the d_{yz} orbital from the $Ru(NH_3)_4$ fragment and π* orbital (LUMO, #41 of (qH_2·$catH_4$) free ligand) of the bridging ligand localized on the qH_2 end and contains substantial Ru d character. Thus there are components of the $d(t_{2g})$ orbitals from $[Ru(NH_3)_4]^{2+}$ in energy both below and above the $[Ru(bpy)_2]^{2+}$ $d(t_{2g})$ orbitals (Table 3, Fig. 8).

The observation of Ru $d(t_{2g})$ NH_3 lying appreciably below Ru $d(t_{2g})$ bpy is surprising since the former Ru is easier to oxidise than the latter.[27] This must reflect the relative stability of the resulting Ru(III) species; a DFT calculation gave a similar result which is being further analysed.

(c) (qH_2·qH_2) Oxidation state. In this oxidation state the coupling is very extensive between metal d_π and both ligand π and π* orbitals. There is also extensive coupling across the bridge since the dihedral angle at the bridge is essentially zero. However conjugation through the bridge to connect the two ruthenium atoms can only proceed through the '*meta*' =NH groups. In the *symmetric* species of assumed symmetry C_{2h}, the d_π orbitals of the two Ru centres are coupled by mixing with the ligand a_u and b_g orbitals. Indeed, the d-orbital density of the six t_{2g} orbitals of the two metal centres is distributed over at least 10 orbitals from LUMO + 1 to HOMO − 8 (#79 to #69) (Table 3, Fig. 8). The HOMO − 3 and HOMO − 4 (#74,73) are the σ $d_{x^2-z^2}$ orbital combinations which are almost pure d

Table 3 Percentage mixing in the symmetric and asymmetric dinuclear complexes in their different states of protonation and oxidation

$[(Ru(NH_3)_4)_2(catH_4{\cdot}catH_4)]^{4+}$

Orbital	%Ru(A1)	%Ru(A2)	%Bridge	$\%NH_3$	Energy/eV
73	0.5	0.5	99	0	−18.183
74	95	0	2	3	−17.575
75	0	95	2	3	−17.574
76	32	63	2	3	−17.511
77	63	31	3	3	−17.509
78	55	40	3	2	−17.469
79 (HOMO)	40	55	3	2	−17.465
80	0	0	100	0	−9.548
81	0	0	100	0	−9.317
82	0	0	100	0	−9.139
83	0	0	100	0	−9.01

$[(Ru(NH_3)_4)_2(qH_2{\cdot}catH_4)]^{4+}$

Orbital	%(Ru(A/qH_2)	%Ru(A/$catH_4$)	%Bridge	$\%NH_3$	Energy/eV	Description[a]
72	19	0	80	1	−18.511	$(d_{yz} + d_{xy})$(Ru-qH_2) + π
73	94	0	3	3	−17.853	d_σ(Ru-qH_2)
74	0	95	2	3	−17.617	d_{yz}(Ru-$catH_4$)
75	47	27	25	1	−17.582	$(d_{yz} - d_{xy})$(Ru-qH_2) + d_{xy}(Ru-$catH_4$)
76	19	68	10	3	−17.551	$(d_{yz} - d_{xy})$(Ru-qH_2) − d_{xy}(Ru-$catH_4$)
77	2	93	3	2	−17.516	d_σ(Ru-$catH_4$)
78 (HOMO)	61	2	35	2	−17.412	$(d_{yz} + d_{xy})$(Ru-qH_2) − π
79	20	0	79	1	−12.035	π* − d_{yz}(Ru-qH_2)
80	0	0	100	0	−9.738	
81	0	0	100	0	−9.357	
82	0	0	100	0	−8.983	

$[(Ru(NH_3)_4)_2(qH_2{\cdot}qH_2)]^{4+}$

Orbital	%Ru(A1)	%Ru(A2)	%Bridge	$\%NH_3$	Energy/eV	Description symmetry
69	5	5	87	3	−20.762	$(d_{yz} - d'_{yz})$ + π, b_g
70	8	8	84	1	−19.191	$(d_{xy} - d'_{xy})$ + π, a_u
71	13	13	73	1	−18.768	$(d_{xy} + d'_{xy})$ + π, b_g
72	33	34	31	2	−17.964	$\{(d_{yz} + d_{xy}) + (d'_{yz} - d'_{xy})\}$ + π, a_u
73	49	45	4	2	−17.949	$(d_\sigma - d'_\sigma)$, b_u
74	45	49	4	2	−17.947	$(d_\sigma + d'_\sigma)$, a_g
75	36	36	26	2	−17.647	$\{(d_{yz} - d_{xy}) - (d'_{yz} + d'_{xy})\}$ + π, b_g
76	36	36	26	2	−17.575	$(d_{xy} - d'_{xy})$ − π, a_u
77 (HOMO)	28	28	42	2	−17.339	$\{(d_{yz} + d_{xy}) - (d'_{yz} - d'_{xy})\}$ − π, b_g
78	12	12	75	1	−12.367	π* − $(d_{yz} + d'_{yz})$, a_u
79	9.5	9.5	80	1	−11.893	π* − $(d_{yz} - d'_{yz})$, b_g
80	0.5	0.5	99	0	−9.757	a_u
81	0	0	100	0	−9.074	b_g

$[Ru(NH_3)_4(catH_4{\cdot}catH_4)Ru(bpy)_2]^{4+}$

Orbital	%Ru(A)	%Ru(bpy)	%Bridge	%bpy	$\%NH_3$	Energy/eV
113	31	0	67	0	2	−17.297
114	92	0	5	0	3	−17.291
115	72	0	26	0	2	−17.210
116	90	0	8	0	2	−17.172
117	0	2	0	98	0	−16.715
118	0	2	0	98	0	−16.608
119	0	84	1	15	0	−15.496
120	0	81	1	18	0	−15.444
121 (HOMO)	0	74	1	25	0	−15.266
122	0	0	100	0	0	−9.133
123	0	2	1	97	0	−9.072
124	0	6	0	93	1	−8.946
125	0	0	100	0	0	−8.785

$[Ru(NH_3)_4(qH_2{\cdot}catH_4)Ru(bpy)_2]^{4+}$

Orbital	%Ru(A)	%Ru(bpy)	%Bridge	%bpy	$\%NH_3$	Energy/eV	Description[b]
112	27	0	72	0	1	−17.883	$(d_{yz} + d_{xy})$ + π, Ru(A)
113	94	0	3	0	3	−17.479	d_σ, RuA
114	67	0	31	0	2	−17.175	$(d_{yz} - d_{xy})$ − π, Ru(A)
115	50	0	50	0	0	−16.961	d_{xy} − π, Ru(A)
116	0	2	0	98	0	−16.782	
117	0	2	0	98	0	−16.653	
118	0	85	1	14	0	−15.594	d_{xy}, Ru(bpy)
119	0	79	1	19	1	−15.480	d_{yz}, Ru(bpy)
120 (HOMO)	0	73	1	26	0	−15.326	d_σ, Ru(bpy)

Table 3 (*Contd.*)

$[Ru(NH_3)_4(qH_2{\cdot}catH_4)Ru(bpy)_2]^{4+}$							
Orbital	%Ru(A)	%Ru(bpy)	%Bridge	%bpy	$\%NH_3$	Energy/eV	Description[b]
121	19	0	80	1	0	−11.649	$\pi^* - d_{yz}$, Ru(A)
122	0	0	72	28	0	−9.150	
123	0	1	27	72	0	−9.135	
124	0	6	0	93	1	−9.006	
$[Ru(NH_3)_4(qH_2{\cdot}qH_2)Ru(bpy)_2]^{4+}$							
Orbital	%Ru(A)	%Ru(bpy)	%Bridge	%bpy	$\%NH_3$	Energy/eV	Description[c]
110	15	0	76	9	0	−18.318	
111	19	4	69	6	1	−17.659	$(d_{yz} + d_{xy})$, Ru(A)
112	94	0	3	0	2	−17.349	d_σ(RuA)
113	54	4	35	5	2	−17.088	$d_{yz} + \pi$, Ru(A)
114	47	3	22	26	1	−16.957	d_{xy}(Ru(A))
115	12	2	12	74	0	−16.906	
116	3	1	3	92	0	−16.821	
117	0	62	23	15	0	−16.026	
118	0	67	7	27	0	−15.989	
119 (HOMO)	3	51	34	12	0	−15.935	
120	18	3	77	1	1	−11.583	$\pi^* - d_{yz}$(Ru(A))
121	1	25	67	7	0	−10.727	$\pi^* - d_{yz}$(Ru(bpy))
122	0	4	2	94	0	−9.277	

[a] Approximate description due to low symmetry. Symmetry with respect to the bridge indicated. [b] Due to the low symmetry, these labels are approximate descriptions; the RuA and Ru(bpy) indicate upon which ruthenium atom the d orbital resides. [c] Approximate description with respect to the bridge. The orientations of orbitals #117–#119 are distorted by interaction with the bpy residues and do not have a simple symmetrical relationship to the bridge.

orbitals (Fig. 7). The energy separation between these in- and out-of-phase combinations is essentially zero (Table 3).

One can identify the $(d_{xy} \pm d'_{xy})$ combinations at (#70,71,76) (Table 3) and the $\{(d_{yz} + d_{xy}) \pm (d'_{yz} - d'_{xy})\}$ combinations at (#72,77) separated by 5040 cm^{-1}, clearly large due to the conjugated pathway. While the $\{(d_{yz} - d_{xy}) - (d'_{yz} + d'_{xy})\}$ combination can be discerned (#75), the corresponding $\{(d_{yz} - d_{xy}) + (d'_{yz} + d'_{xy})\}$ was not evident. There is clearly very extensive coupling through the various orbital pathways *via* the bridging ligand but the presence of so many ligand π and π* orbitals of the same symmetry makes it very difficult to extract actual electronic coupling matrix elements. This is left for future analysis.[31]

However comparison of the MOs of the free ligand (Fig. 5) with those of the complex reveals that the low lying orbitals #70,71 are combinations of the d orbitals primarily with free ligand orbitals #38,39 respectively, while the orbitals #72,78 involve d primarily with ligand orbital #40, and the complex pair #75,79 primarily with ligand orbital #41. These orbital combinations are recognizable though clearly there must be additional mixing between orbitals of the same symmetry.

The alternative C_{2v} bridge conformation yields data (spectroscopic transition energies, *etc.*) which do not differ significantly from the C_{2h} conformation. A calculation for the symmetric $(qH_2{\cdot}qH_2)$ species but with a dihedral angle of 90° yielded a predicted electronic spectrum in poorer agreement with the experimental spectrum than the zero degree dihedral angle calculation.

In the *asymmetric* species the mixing is extensive and complex, however it only occurs between individual metal centres and the bridging ligand. There is a large energetic difference between the $d(t_{2g})$ orbitals of the $[Ru(NH_3)_4]^{2+}$ fragment and the $[Ru(bpy)_2]^{2+}$ fragment,[1] which inhibits their mixing.

The HOMO–HOMO − 2 (#119–#117) orbitals contain the t_{2g} set of the $[Ru(bpy)_2]^{2+}$ fragment mixed extensively with bpy and to a varying degree with the bridging ligand π and π* orbitals. Thus HOMO − 1 (#118) has σ-symmetry with respect to the bridge and is only minimally mixed therewith (Table 3, Fig. 8). The LUMO is primarily a π*-bridge orbital coupled to the d_{yz} of the $[Ru(NH_3)_4]^{2+}$ fragment and the LUMO + 1 is a π*-bridge orbital coupled to the d_{yz} of the $[Ru(bpy)_2]^{2+}$ fragment, both with substantial metal $d(t_{2g})$ character.

The t_{2g} set of the $[Ru(NH_3)_4]^{2+}$ fragment is distributed (> 12% in each orbital) over HOMO − 4 to HOMO − 9 (#115–#110) and the LUMO. HOMO − 3 and HOMO − 4 are predominantly bpy orbitals. Table 3 shows the descriptions of each MO although in this low symmetry molecule, it is not always possible to make a simple identification of the d orbital involved. However (#110) and (#113) appear to be the bonding and anti-bonding interactions of a d orbital with a π-orbital respectively, and (#112) is clearly the σ-symmetry orbital with little coupling to the bridge. Clearly there is extensive coupling of both sets of metal d_π levels to the π and π* orbitals of the ligand bridge, as in the symmetric $(qH_2{\cdot}qH_2)$ species but coupling between the metal ions across the bridge is minimal.

(d) Ruthenium(III) species. The ruthenium(III) species are not very stable and were not isolated. The mixed valence $[Ru^{III}(qH_2{\cdot}qH_2)Ru^{II}]$ species may, in principle, be localised or delocalised and may be flat or twisted at the central C–C bridge. Since we were not able to collect much data on these species, we do not attempt to calculate them at present.

Relative orbital energies

The relative orbital energies are listed in Table 3 and displayed in Fig. 9 and 10. As anticipated the spread in the $d(t_{2g})$ orbitals is quite small when the metal is attached to the unmixed $catH_4$ end of the $(catH_4{\cdot}catH_4)$ or $(qH_2{\cdot}catH_4)$ species. However the splitting of the $d(t_{2g})$ set attached to the qH_2 fragment is significantly larger.

In the asymmetric species, the energies of localized bpy orbitals remain essentially constant and the overall splitting of the Ru $d(t_{2g})$ bpy levels attached to qH_2 remains much smaller than for the corresponding Ru $d(t_{2g})$ NH_3 fragment. Competition for a d_π orbital interaction between the bpy and bridge ligands may then cause less effective overlap with the bridge than is present with the tetrammine ruthenium centre.

Electronic spectra

Spectroscopic data are listed in Table 4 for both the experimental and the calculated spectra. Assignments of the spectra, based on the ZINDO/S calculations and orbital mixing, follow.

(i) Symmetric species. *(a)* $[(Ru(NH_3)_4)_2(catH_4{\cdot}catH_4)]^{4+}$. This species has a simple electronic spectrum (Fig. 3, spectrum 0) lacking intense absorption in the visible region. The ZINDO/S analysis predicts that there are no intense transitions in the visible region for this complex. However a weak feature near 29400 cm^{-1} is reasonably assigned as a d–d transition ($d_\sigma(t_{2g}) \longrightarrow d_{\sigma*}$) and two transitions in the UV are identified as MLCT and π–π* transitions with energies well reproduced by the ZINDO calculation (Table 4). Certainly these spectra are completely in accord with the formulation of this species as the fully reduced ($catH_4{\cdot}catH_4$) redox isomer.

(b) $[(Ru(NH_3)_4)_2(qH_2{\cdot}catH_4)]^{4+}$. The electronic spectrum of this complex is shown in Fig. 3, spectrum 2. Here we anticipate a strong visible region MLCT transition between the d + π* ⟶ π* − d orbitals and the band at 20160 cm^{-1} is so assigned (#75 ⟶ #79). At higher energies there are a series of predicted MLCT and π ⟶ π* transitions which reproduce the general experimental features although not all the predicted bands are resolved experimentally. The strong visible region band confirms the presence of a qH_2 oxidation fragment.

(c) $[(Ru(NH_3)_4)_2(qH_2{\cdot}qH_2)]^{4+}$. The electronic spectrum (Table 4) of this complex is shown in Fig. 3, spectrum 4. This complex is assumed to have C_{2h} symmetry, and the observed electronic transitions are Laporte allowed. An even more intense visible region band is predicted than for the ($qH_2{\cdot}catH_4$) species because the number of qH_2 chromophores has doubled; otherwise the assignment will be similar. The first transition is to ^1B_u calculated to be at 20080 cm^{-1} (experimentally 19690 cm^{-1}) and is a mixture of the #75 and #77 to LUMO (#78) ($b_g \longrightarrow a_u$) transitions. These transitions involve very highly mixed orbitals, with scrambled d components and are MLCT transitions, with π ⟶ π* character. Transition to LUMO + 1 (#79) from #76 produces another ^1B_u MLCT state seen as a shoulder, while a more intense feature at 33780 cm^{-1} is yet another ^1B_u MLCT state terminating on bridge orbital #80. The overall agreement between predicted and experimental band energies is good.

Compared with the corresponding band in the symmetric ($qH_2{\cdot}catH_4$) species, the oscillator strength of the visible region MLCT band does double in value, and shifts to the red probably because of greater delocalisation.

(d) Ruthenium(III) species. Data for the two Ru^{III} species are included in Table 4 (Fig. 3 inset) but for reasons noted above, we have not obtained any calculated data. The broad shoulder on the low energy side of the mixed valence species is reasonably assigned to the inter-valence transition.

(ii) Asymmetric species. *(a)* $[Ru(NH_3)_4(catH_4{\cdot}catH_4)Ru(bpy)_2]^{4+}$. The spectra of the asymmetric species are more complex than the symmetric species because they have C_1 symmetry and there is also the complication of having the $[Ru(bpy)_2]^{2+}$ chromophore which has electronic transitions of its own (see Fig. 4, spectrum 0). Clearly the visible region absorption can only be $Ru(d_\pi) \longrightarrow \pi^*$ (1) (bpy) in character (Table 4). A shoulder to higher energy is associated with the expected [1–6] $Ru(d_\pi) \longrightarrow \pi^*$ (2) (bpy) transitions (orbitals #126–#129).

(b) $[Ru(NH_3)_4(qH_2{\cdot}catH_4)Ru(bpy)_2]^{4+}$. The oxidation of one end of the bridging ligand creates a new chromophore in the $(NH_3)_4Ru(qH_2)$ end of the molecule (see Fig. 4, spectrum 2) and we now anticipate two visible region transitions corresponding to MLCT to bpy and to the bridge. These are indeed observed, lying fairly close together. The lower energy visible region transition involves orbitals (#114,115 ⟶ #121) that are localized on the $(NH_3)_4Ru(qH_2)$ end of the molecule being $d(t_{2g})$ $(NH_3)_4Ru \longrightarrow \pi^*$ (LUMO) qH_2 MLCT transition with some π ⟶ π* character. The higher energy component is then the $Ru(d_\pi) \longrightarrow \pi^*$(bpy) set of transitions as calculated (Table 4). These MLCT transitions to bipyridine are calculated to be very much weaker than the $RuA(d_\pi) \longrightarrow qH_2(\pi^*)$ MLCT transition. Indeed the actual ($Ru(d_\pi) \longrightarrow \pi^*$(bpy)) shoulder on the high energy side of the visible region band is actually quite weak, being built upon the high energy tail of the lower energy transition. Its reported experimental intensity in Table 4 is then a dramatic overestimate of its true (deconvoluted) intensity. At higher energy lie the expected $d(t_{2g}) \longrightarrow \pi^*(2)$ bpy MLCT transitions, some additional MLCT to the bridge and π–π* transitions (Table 4).

(c) $[Ru(NH_3)_4(qH_2{\cdot}qH_2)Ru(bpy)_2]^{4+}$. In this oxidation state there are many chromophores and many possible transitions (Fig. 4, spectrum 4). Clearly we can expect two different $Ru(d_\pi) \longrightarrow$ bridge in addition to the $Ru(d_\pi) \longrightarrow \pi^*$ (bpy) bands. The increasing oxidation on the bridge causes the ruthenium atoms to be more positive and this shifts the $Ru(d_\pi) \longrightarrow \pi^*$(bpy) bands to higher energy where they appear as a shoulder near 430 nm (Fig. 4).

The strong visible region band is assigned to the HOMO ⟶ LUMO transition which is a complex transition containing MMCT, MLCT and π ⟶ π* components as seen from the nature of these MOs in Table 3. Additional MLCT transitions from lower lying d orbitals to the LUMO appear more weakly at higher energy and are responsible for the broad absorption near 24000 cm^{-1}. The corresponding MLCT transitions to LUMO + 1 are weaker and at higher energy (Table 4). The anticipated $Ru(d_\pi) \longrightarrow \pi^*$ (bpy) transitions appear at rather higher energies due to the high net oxidation state of the complex.

The overall agreement in this series of six complexes between the observed experimental spectra and the ZINDO calculated spectra is remarkably good, with the poorest agreement perhaps with the asymmetric ($qH_2{\cdot}qH_2$) species.

Conclusions

This paper has described the synthesis of two new dinuclear complexes, and the spectroscopic characterization of the two- and four-electron oxidized products. A ZINDO/S analysis of the closed shell Ru(II) complexes produced a reasonable fit to the experimentally determined spectra providing confidence in the significance of the electronic structural analysis. The ZINDO/S analysis reveals in considerable detail the extensive metal–ligand orbital mixing that exists in many of these complexes. As would be anticipated the ($qH_2{\cdot}qH_2$) species are by far the most mixed and the ($catH_4{\cdot}catH_4$) are the least mixed. The extent of the mixing in the ($qH_2{\cdot}qH_2$) species is further evidence of the close orbital energy match and the good overlap that occurs in this type of complex.

The mixing in these species can be described using the familiar terminology of back-donation. Species such as 2,2′-bipyridine are regarded as good π-back bonding ligands but the extent of π-back bonding in such species is very much less than observed here with the qH_2 fragments. Back-donation in the 2,2′-bipyridine ruthenium species involves mixing between metal d_π into π* (bpy) ligands of the order of 5–10% at most, corresponding to a formal transfer of 0.1–0.2 electrons. In the qH_2 species we commonly observe *ca.* 20% admixture [1a,5d,9] or a formal transfer of 0.4 electrons. Indeed in the dinuclear $qH_2{\cdot}qH_2$ complex, we observe around 0.4 electron back donation from each end of the molecule for a total of approximately 0.8 electrons into the flat π* LUMO and LUMO + 1 of $qH_2{\cdot}qH_2$.

Unfortunately it has so far not proved possible to obtain crystals of these species for X-ray analysis—this is still being attempted. The extent to which the optimized ZINDO/1 struc-

Table 4 Electronic spectroscopic data for this series of complexes and related complexes in 0.1 M aqueous H_3PO_4

Energy[a]/cm^{-1}	Calculated energy/cm^{-1} (f)[b]	Assignment
$[(Ru(NH_3)_4)_2(catH_4{\cdot}catH_4)]^{4+}$ (HOMO = 79)		
47620	47900 (0.44)	$\pi \longrightarrow \pi^*$; 72 $\longrightarrow$ 81
39370 (4.25, 8010, 0.62)	39680 (0.10)	$\pi \longrightarrow \pi^*$; MLCT, 77 $\longrightarrow$ 80 and 76 $\longrightarrow$ 81
29410 (sh) (3.29)	30710 (0.0002)	d $\longrightarrow$ d transitions, 79 $\longrightarrow$ 86 and 87
$[(Ru(NH_3)_4)_2(qH_2{\cdot}catH_4)]^{4+}$ (HOMO = 78)		
47620	48450 (0.54)	$\pi \longrightarrow \pi^*$, 69 $\longrightarrow$ 79
	46700 (0.14)	$\pi \longrightarrow \pi^*$; MLCT, 78 $\longrightarrow$ 81
	42300 (0.17)	$\pi \longrightarrow \pi^*$; MLCT, 78 $\longrightarrow$ 82
40000 (sh)	41450 (0.15)	$\pi \longrightarrow \pi^*$; MLCT, 75 $\longrightarrow$ 82
34300 (4.12, 7360, 0.42)	36950 (0.64)	$\pi \longrightarrow \pi^*$, MLCT, 78 $\longrightarrow$ 81
	36900 (0.1)	d $\longrightarrow$ d; LMCT, 78 $\longrightarrow$ 86
	33170 (0.1)	$\pi \longrightarrow \pi^*$, d $\longrightarrow$ d, 73 $\longrightarrow$ 84 and 70 $\longrightarrow$ 79
28600 (sh)	24230 (0.04)	$\pi \longrightarrow \pi^*$; MLCT, 70 and 72 $\longrightarrow$ 79
20160 (4.01, 3740, 0.17)	21540 (0.64)	MLCT; $\pi \longrightarrow \pi^*$, 75 $\longrightarrow$ 79
$[(Ru(NH_3)_4)_2(qH_2{\cdot}qH_2)]^{4+}$ (HOMO + 77)		
40650 (sh)	41780 (0.43)	MLCT; $\pi \longrightarrow \pi^*$, 76 $\longrightarrow$ 81, 75 $\longrightarrow$ 82
	39500 (0.13)	MLCT; $\pi \longrightarrow \pi^*$, 75 $\longrightarrow$ 80
	37800 (0.07)	$\pi \longrightarrow \pi^*$; MLCT, 71 $\longrightarrow$ 78, 70 $\longrightarrow$ 79
33780 (4.24, 9960, 0.75)	36220 (0.77)	$\pi \longrightarrow \pi^*$; MLCT, 77 $\longrightarrow$ 80
28600 (sh)	29470 (0.20)	$\pi \longrightarrow \pi^*$; MLCT, 76 $\longrightarrow$ 79
19690 (4.27, 4950, 0.40)	20080 (1.38)	$\pi \longrightarrow \pi^*$; MLCT, 77 and 75 $\longrightarrow$ 78
$[Ru(NH_3)_4(catH_4{\cdot}catH_4)Ru(bpy)_2]^{4+}$ (HOMO = 121)		
41100 (4.61)	42000 (0.14)	Ru $\longrightarrow$ bpy, MLCT, 120 $\longrightarrow$ 134, 121 $\longrightarrow$ 135
39100 (sh)	37400 (0.45)	Ru $\longrightarrow$ bpy, MLCT, 120 $\longrightarrow$ 132
	36500 (0.55)	119 $\longrightarrow$ 131
	36200 (0.36)	120 $\longrightarrow$ 131, 121 $\longrightarrow$ 132
34400 (4.82, 3300, 1)	34720 (0.23)	Ru $\longrightarrow$ bpy, MLCT, 121 $\longrightarrow$ 131
	33040 (0.12)	Ru(bpy) $\longrightarrow$ bridge, MLCT, 121 $\longrightarrow$ 126
	32760 (0.1)	Ru(bpy) $\longrightarrow$ bridge, MLCT, 121 $\longrightarrow$ 126
28300 (sh)		Ru $\longrightarrow$ bpy, MLCT
	31990 (0.23)	121 $\longrightarrow$ 127
	31300 (0.18)	121 $\longrightarrow$ 128 and 129
23500 (sh)		Ru $\longrightarrow$ bpy, MLCT
20680 (4.14)	23370 (0.13)	119 $\longrightarrow$ 123
	23120 (0.05)	120 $\longrightarrow$ 124
	21760 (0.03)	121 $\longrightarrow$ 123
$[Ru(NH_3)_4(qH_2{\cdot}catH_4)Ru(bpy)_2]^{4+}$ (HOMO = 120)		
41100 (4.55)		
39100 (sh)		
34400 (4.75, 4000, 1)	33000 (0.12)	Ru $\longrightarrow$ bpy, MLCT, 118 $\longrightarrow$ 128, 120 $\longrightarrow$ 131
28300 (sh)	32520 (0.12)	Ru $\longrightarrow$ bpy, MLCT, 119 $\longrightarrow$ 127, 118 $\longrightarrow$ 128
	32500 (0.13)	$\pi \longrightarrow \pi^*$ bridge, 107 and 111 $\longrightarrow$ 121
	31880 (0.23)	Ru $\longrightarrow$ bpy, MLCT, 120 $\longrightarrow$ 127
	31400 (0.12)	$\pi \longrightarrow \pi^*$ bridge, 111 $\longrightarrow$ 121
	31340 (0.10)	Ru $\longrightarrow$ bpy, MLCT, 120 $\longrightarrow$ 128
(*c*)	24200 (0.14)	$Ru(NH_3)_4 \longrightarrow$ bridge; MLCT, 112 $\longrightarrow$ 121
20300 (4.14)		Ru $\longrightarrow$ bpy, MLCT
	23400 (0.06)	118 $\longrightarrow$ 123
	23000 (0.09)	119 $\longrightarrow$ 124
18420 (4.19, 3440, 0.25)	21250 (0.75)	$Ru(NH_3)_4 \longrightarrow$ bridge; $\pi \longrightarrow \pi^*$; MLCT, 115 and 114 $\longrightarrow$ 121
$[Ru(NH_3)_4(qH_2{\cdot}qH_2)Ru(bpy)_2]^{4+}$ (HOMO = 119)		
40000 (sh)	Many transitions	
34600	34900 (0.25)	117 $\longrightarrow$ 127
	34200 (0.68)	119 $\longrightarrow$ 124
	32400 (0.06)	π(bpy) $\longrightarrow \pi^*$(bridge) + Ru(bpy) + $Ru(NH_3)$, LLCT, LMCT, 116 $\longrightarrow$ 120 and 121
	32240 (0.32)	$\pi \longrightarrow \pi^*$ bpy, 116 $\longrightarrow$ 123 and 115 $\longrightarrow$ 122
	31670 (0.13)	$\pi \longrightarrow \pi^*$ bpy, 116 $\longrightarrow$ 120 and 122
28000 (sh)	26520 (0.12)	$Ru(bpy)_2 \longrightarrow$ bpy π^* MLCT, 118 $\longrightarrow$ 122
23800 (3.89)	25600 (0.05)	115 $\longrightarrow$ 121, bpy $\longrightarrow$ bridge, LLCT
	23670 (0.10)	$Ru(NH_3)_4 \longrightarrow$ bridge, $\pi \longrightarrow \pi^*$; MLCT, 113 $\longrightarrow$ 120
	22470 (0.27)	$Ru(bpy)_2 \longrightarrow$ bridge; $\pi \longrightarrow \pi^*$ bridge, 117 $\longrightarrow$ 120
18300 (4.33, 4600, 0.45)	17500 (1.37)	$Ru(bpy)_2(qH_2) \longrightarrow Ru(NH_3)_4(qH_2)$, 119 $\longrightarrow$ 120
14000 (sh)	11000 (0.01)	$Ru(NH_3)_4$, π-bpy, π-bridge $\longrightarrow Ru(NH_3)_4(qH_2)$, 114 $\longrightarrow$ 120
$[(Ru(bpy)_2)_2(qH_2{\cdot}qH_2)]^{4+}$ (HOMO = 161)[4,32]		
23050	21370 (0.35)	$(bpy)_2Ru \longrightarrow$ bridge, 161 $\longrightarrow$ 163, 156 $\longrightarrow$ 162
17100	17870 (1.29)	$(bpy)_2Ru \longrightarrow$ bridge, 161 and 159 $\longrightarrow$ 162

Table 4 (*Contd.*)

Energy[a]/cm^{-1}	Calculated energy/cm^{-1} (f)[b]	Assignment
$[(Ru(NH_3)_4)_2(qH_2{\cdot}qH_2)]^{5+}$		
34700 (4.19)		
21700 (4.18)		MLCT and LMCT
18100 (sh) (4.09)		Intervalence MMCT?
$[(Ru(NH_3)_4)_2(qH_2{\cdot}qH_2)]^{6+}$		
34300 (sh) (4.13)		
22400 (4.13)		LMCT

[a] Data in parentheses are (log (ε/dm^3 mol^{-1} cm^{-1}), half band width (cm^{-1}), oscillator strength). [b] Principal calculated bands in the visible and near-UV region with calculated oscillator strengths (in parentheses) >0.05. [c] A broad background absorption is evident in this region, see Fig. 3, insert.

tures are close to the real structures still remains to be assessed. However the overall features of the structures, including bond distance, are most likely correct and the uncertainty remains primarily with the twist angle at the biphenyl link. Small changes in the twist angle have no substantive effect on the descriptions of the molecules discussed here. In particular the extent of interaction between the metal centre and its local diimino fragment is not greatly affected by the twist angle.

Acknowledgements

We would like to thank Drs Elaine Dodsworth, Yu-Hong Tse, Hitoshi Masui, Carlos da Cunha, and Mr Sergei I. Gorelsky for valuable discussion. Thanks are also due to Professor Michael Siu and his students for assistance with the electrospray mass spectroscopy. We would also like to thank CNPq (Conselho de Desenvolvimento Cientifico e Tecnológico da Secretaria de Ciência e Tecnologia do Brasil), and the Natural Sciences and Engineering Research Council of Canada (Ottawa) for financial support. Some of the $RuCl_3$ used in this project was a generous loan from Johnson Matthey Co. Inc.

References

1 (*a*) R. A. Metcalfe and A. B. P. Lever, *Inorg. Chem.*, 1997, **36**, 4762; (*b*) R. A. Metcalfe, E. S. Dodsworth, S. S. Fielder, D. J. Stufkens, A. B. P. Lever and W. J. Pietro, *Inorg. Chem.*, 1996, **35**, 7741; (*c*) R. A. Metcalfe, Ph.D. Thesis, York University, Canada, 1988.
2 C. J. da Cunha, S. S. Fielder, D. V. Stynes, H. Masui, P. R. Auburn and A. B. P. Lever, *Inorg. Chim. Acta.*, 1996, **242**, 293.
3 R. A. Metcalfe, E. S. Dodsworth, W. J. Pietro, A. B. P. Lever and D. J. Stufkens, *Inorg. Chem.*, 1993, **32**, 3581.
4 P. R. Auburn and A. B. P. Lever, *Inorg. Chem.*, 1990, **29**, 2551.
5 (*a*) H. Masui, A. B. P. Lever and P. R. Auburn, *Inorg. Chem.*, 1991, **30**, 2402; (*b*) H. Masui, A. B. P. Lever and E. S. Dodsworth, *Inorg. Chem.*, 1993, **32**, 258; (*c*) H. Masui, Ph.D. Thesis, York University, Canada, 1994; (*d*) H. Masui, A. L. Freda and A. B. P. Lever, *Inorg. Chem.*, submitted; (*e*) C. J. da Cunha, E. S. Dodsworth, M. A. Monteiro and A. B. P. Lever, *Inorg. Chem.*, 1999, **38**, in the press.
6 P. Belser, A. von Zelewsky and M. Zehnder, *Inorg. Chem.*, 1981, **20**, 3098; H. Y. Cheng and S. M. Peng, *Inorg. Chim. Acta*, 1990, **169**, 23; E. H. Cutin, N. E. Katz, P. A. M. Williams and P. J. Aymonino, *Transition Met. Chem.*, 1991, **16**, 155; S. Nemeth and L. I. Simandi, *Inorg. Chem.*, 1994, **33**, 5964; G. Ricciardi, A. Rosa, G. Morelli and F. Lelj, *Polyhedron*, 1991, **10**, 955; O. Carugo, K. Djinovic and C. B. Castellani, *J. Chem. Soc.*, *Dalton Trans.*, 1991, 1551; J. Rall, A. F. Stange, K. Hübler and W. Kaim, *Angew. Chem.*, *Int. Ed.*, 1998, **37**, 2681; T. Jüstel, J. Bendix, N. Metzler, T. Weyhermüller, B. Nuber and K. Wieghardt, *Inorg. Chem.*, 1998, **37**, 35; S.-M. Peng, K. Peters, E. M. Peters and A. Simon, *Inorg. Chim. Acta*, 1985, **101**, L35; S. Peng, C. Chen, D. Liaw, C. Chen and Y. Wang, *Inorg. Chim. Acta*, 1985, **101**, L31; L. I. Simandi and S. Nemeth, *Inorg. Chim. Acta*, 1998, **270**, 326.
7 J. F. Joulie, E. Schatz, M. D. Ward, F. Weber and L. J. Yellowlees, *J. Chem. Soc.*, *Dalton Trans.*, 1994, 799; S. Bruni, F. Cariati, A. Dei and D. Gatteschi, *Inorg. Chim. Acta*, 1991, **186**, 157; A. Dei, D. Gatteschi and L. Pardi, *Inorg. Chem.*, 1990, **29**, 1442; M. D. Ward, *Inorg. Chem.*, 1996, **35**, 1712; F. Heinze, S. Mann, G. Huttner and L. Zsolnai, *Chem. Ber.*, 1996, **129**, 1115; A. Dei, D. Gatteschi, L. Pardi and U. Russo, *Inorg. Chem.*, 1991, **30**, 2589; A. Dei, D. Gatteschi and L. Pardi, *Inorg. Chim. Acta*, 1991, **189**, 125; M. A. Calvo, A. M. M. Lanfredi, L. A. Oro, M. T. Pinillos, C. Tejel, A. Tiripicchio and F. Ugozzoli, *Inorg. Chem.*, 1993, **32**, 1147; S. Cueto, H. P. Straumann, P. Rys, W. Petter, V. Gramlich and F. S. Rys, *Acta Crystallogr.*, *Sect. C*, 1992, **48**, 458; A. Elduque, Y. Garces, L. A. Oro, M. T. Pinillos, A. Tiripicchio and F. Ugozzoli, *J. Chem. Soc.*, *Dalton Trans.*, 1996, 2155; R. F. Johnston, P. K. Sengupta, M. B. Ossain, R. Vanderhelm, W. Y. Jeong and R. A. Holwerda, *Acta Crystallogr.*, *Sect. C*, 1990, **46**, 1796; A. Tiripicchio, *Inorg. Chem.*, 1993, **32**, 1147; M. X. Zhang, Z. L. Liu, L. Yang and Y. C. Liu, *J. Chem. Soc.*, *Chem. Commun.*, 1991, 1054; J. Zubieta, *J. Chem. Soc.*, *Chem. Commun.*, 1988, 1017; T. E. Keyes, R. J. Forster, P. M. Jayaweera, C. G. Coates, J. J. McGarvey and J. G. Vos, *Inorg. Chem.*, 1998, **37**, 5925.
8 (*a*) W. P. Anderson, T. Cundari, R. S. Drago and M. C. Zerner, *Inorg. Chem.*, 1989, **29**, 1; (*b*) W. P. Anderson, T. Cundari and M. C. Zerner, *Int. J. Quantum Chem.*, 1991, **39**, 31; (*c*) W. P. Anderson, W. D. Edwards and M. C. Zerner, *Inorg. Chem.*, 1986, **25**, 2728; (*d*) A. D. Bacon and M. C. Zerner, *Theor. Chim. Acta*, 1979, **53**, 21; (*e*) M. C. Zerner, *Metal–Ligand Interactions*, Kluwer Academic Publishers, Dordrecht, 1996, p. 493; (*f*) M. C. Zerner, G. H. Loew, R. F. Kirchner and U. T. Mueller-Westerhoff, *J. Am. Chem. Soc.*, 1980, **102**, 589; (*g*) J. C. Culberson, P. Knappe, N. Rösch and M. C. Zerner, *Theor. Chim. Acta*, 1987, **71**, 21; (*h*) J. Ridley and M. C. Zerner, *Theor. Chim. Acta*, 1973, **32**, 111; (*i*) J. Ridley and M. C. Zerner, *Theor. Chim. Acta*, 1976, **42**, 223.
9 S. I. Gorelsky, E. S. Dodsworth, A. B. P. Lever and A. Vlcek, *Coord. Chem. Rev.*, 1998, **174**, 469.
10 Y. K. Shin, B. S. Brunschwig, C. Creutz, M. D. Newton and N. Sutin, *J. Phys. Chem.*, 1996, **100**, 1104 and references therein; K. J. Lachance-Galang, P. E. Doan, M. J. Clarke, U. Rao, A. Yamano and B. M. Hoffman, *J. Am. Chem. Soc.*, 1995, **117**, 3529; L. T. Zhang and M. Ondrechen, *Inorg. Chim. Acta*, 1994, **226**, 43; O. V. Sizova, V. I. Baranosvskii, N. V. Ivanova and A. B. Nikol'skii, *Russ. J. Gen. Chem.*, 1997, **67**, 1667; O. V. Sizova, V. I. Baranovski, N. V. Ivanova and A. I. Panin, *Int. J. Quantum Chem.*, 1997, **65**, 183; O. V. Sizova, V. I. Baranovskii, N. V. Ivanova and A. I. Panin, *Russ. J. Coord. Chem.*, 1997, **23**, 197; O. V. Sizova, N. V. Ivanova and A. B. Nikolskii, *Zh. Obshch. Khim.*, 1997, **67**, 26; O. V. Sizova, V. I. Baranovski, N. V. Ivanova and A. I. Panin, *Int. J. Quantum Chem.*, 1997, **65**, 183; O. V. Sizova, V. I. Baranovskii, N. V. Ivanova and A. I. Panin, *Russ. J. Coord. Chem.*, 1997, **23**, 197; O. V. Sizova, N. V. Ivanova, A. Y. Ershov, A. B. Nikolskii and I. V. Rogachevskii, *Zh. Obshch. Khim.*, 1997, **67**, 1409; O. V. Sizova, N. V. Ivanova and A. B. Nikolskii, *Zh. Obshch. Khim.*, 1997, **67**, 26; O. V. Sizova, A. I. Panin, N. V. Ivanova and V. I. Baranovskii, *J. Struct. Chem.*, 1997, **38**, 366; Y. K. Shin, D. J. Szalda, B. S. Brunschwig, C. Creutz and N. Sutin, *Inorg. Chem.*, 1997, **36**, 3190; J. Yang, D. Seneviratne, G. Arbatin, A. M. Andersson and J. C. Curtis, *J. Am. Chem. Soc.*, 1997, **119**, 5329; A. Broo and P. Lincoln, *Inorg. Chem.*, 1997, **36**, 2544; H. Rensmo, S. Lunell and H. Siegbahn, *J. Photochem. Photobiol. A: Chem.*, 1998, **114**, 117; O. V. Sizova, V. I. Baranovskii, A. I. Panin, N. V. Ivanova and A. B. Nikolskii, *Zh. Obshch. Khim.*, 1997, **67**, 1611; O. V. Sizova, I. Panin, V. I. Baranovskii, A. B. Nikolskii and N. V. Ivanova, *Zh. Obshch. Khim.*, 1997, **67**, 1761.
11 See, for example: (*a*) S. Ernst, V. Kasack and W. Kaim, *Inorg. Chem.*, 1988, **27**, 1146; (*b*) S. Joss, H. Reust and A. Ludi, *J. Am. Chem. Soc.*, 1981, **103**, 981; (*c*) S. Joss, H. B. Burgi and A. Ludi, *Inorg. Chem.*, 1985, **24**, 949; (*d*) S. Joss, K. M. Hasselbach, H. B. Bürgi, R. Wordel, F. E. Wagner and A. Ludi, *Inorg. Chem.*, 1989, **28**, 1815; (*e*) J. E. B. Johnson, C. Degroff and R. R. Ruminski, *Inorg. Chim. Acta*, 1991, **187**, 7380; (*f*) M. A. S. Aquino, F. L. Lee, E. J. Gabe, C. Bensimon,

J. E. Greedan and R. J. Crutchley, *J. Am. Chem. Soc.*, 1992, **114**, 5130; (*g*) W. Bruns, W. Kaim, E. Waldhor and M. Krejcik, *J. Chem. Soc., Chem. Commun.*, 1993, 1868; (*h*) C. Creutz, M. D. Newton and N. Sutin, *J. Photochem. Photobiol. A*, 1994, **82**, 47; (*i*) H. Y. Huang, W. J. Chen, C. C. Yang and A. Yeh, *Inorg. Chem.*, 1991, **30**, 1862; (*j*) V. Kasack, W. Kaim, H. Binder, J. Jordanov and E. Roth, *Inorg. Chem.*, 1995, **34**, 1924; (*k*) J. A. Roberts and J. T. Hupp, *Inorg. Chem.*, 1992, **31**, 157; (*l*) M. D. Ward, *Chem. Soc. Rev.*, 1995, **24**, 121; (*m*) A. E. Almaraz, L. A. Gentil, L. M. Baraldo and J. A. Olabe, *Inorg. Chem.*, 1997, **36**, 1517; (*n*) J. F. Endicott, M. A. Watzky, X. Q. Song and T. Buranda, *Coord. Chem. Rev.*, 1997, **159**, 295; (*o*) F. Salaymeh, S. Berhane, R. Yusof, R. de la Rosa, E. Y. Fung, R. Matamoros, K. W. Lau, Q. Zheng, E. M. Kober and J. C. Curtis, *Inorg. Chem.*, 1993, **32**, 3895.

12 D. D. Perrin, W. L. F. Armarego and D. R. Perrin, *Purification of Laboratory Chemicals*, Pergamon Press, Elmsford, New York, 2nd edn., 1980.

13 A. B. P. Lever, E. R. Milaeva and G. Speier, *Phthalocyanines: Properties and Applications*, eds. C. C. Leznoff and A. B. P. Lever, VCH, New York, 1995, vol. 3, p. 3.

14 S. I. Gorelsky and A. B. P. Lever, unpublished work.

15 K. Krogh-Jespersen, J. D. Westbrook, J. A. Potenza and H. J. Schugar, *J. Am. Chem. Soc.*, 1987, **109**, 7025.

16 A. Szabo and N. S. Ostlund, *Modern Quantum Chemistry*, Macmillan Publ. Co., New York, 1982.

17 X. Cheng, Q. Gao, R. D. Smith, E. E. Simanek, M. Mammen and G. M. Whitesides, *J. Org. Chem.*, 1996, **61**, 2204; J. Manna, J. A. Whiteford, P. J. Stang, D. C. Muddiman and R. D. Smith, *J. Am. Chem. Soc.*, 1996, **118**, 8731; G. J. Langley, E. Hecquet, I. P. Morris and D. G. Hamilton, *Rapid Commun. Mass Spectrom.*, 1997, **11**, 165; A. Marquis-Rigault, A. Dupont-Gervais, A. Van Dorsselaer and J.-M. Lehn, *Chem. Eur. J.*, 1996, **2**, 1395; D. P. Funeriu, J.-M. Lehn, G. Baum and D. Fenske, *Chem. Eur. J.*, 1997, **3**, 99; C. Moucheron, A. Kirsch-De Mesmaeker, A. Dupont-Gervais, E. Leize and A. Van Dorsselaer, *J. Am. Chem. Soc.*, 1996, **118**, 12834; B. C. Gilbert, N. W. J. Kamp, J. R. Lindsay Smith and J. Oakes, *J. Chem. Soc., Perkin Trans. 2*, 1998, 1841; W. Henderson, J. S. McIndoe, B. K. Nicholson and P. J. Dyson, *J. Chem. Soc., Dalton Trans.*, 1998, 519; C. Jiang, W. Henderson, T. S. A Hor, L. J. McCaffrey and Y. K. Yan, *Chem. Commun.*, 1998, 2029; A. S. Batsanov, A. V. Churakov, M. A. M. Easson, L. J. Govenlock, J. A. K. Howard, J. M. Moloney and D. Parker, *J. Chem. Soc., Dalton Trans.*, 1999, 323; M. J. Deery, O. W. Howarth and K. R. Jennings, *J. Chem. Soc., Dalton Trans.*, 1997, 4783; G. Hopfgartner, C. Piguet and J. D. Henion, *J. Am. Soc. Mass Spectrom.*, 1994, **5**, 748; C. Piguet, G. Bernardelli and H. Hopfgartner, *Chem. Rev.*, 1997, **97**, 2005; K. A. Hirsch, S. R. Wilson and J. S. Moore, *J. Am. Chem. Soc.*, 1997, **199**, 10401.

18 I. K. Chu, T.-C. Lau and K. W. M. Siu, *J. Mass Spectrom.*, 1998, **33**, 811.

19 C. G. Kuehn and H. Taube, *J. Am. Chem. Soc.*, 1976, **98**, 689; B. P. Sullivan, D. J. Salmon and T. J. Meyer, *Inorg. Chem.*, 1978, **17**, 3334.

20 S. Diamond, Ph.D Thesis, Stanford University, 1975.

21 L. Vasconcellos, R. A. Metcalfe, H. Mirza and A. B. P. Lever, to be published.

22 J. K. M. Sanders and B. K. Hunter, *Modern NMR Spectroscopy, A Guide for Chemists*, Oxford University Press, New York, 1978; J. B. Lambert, H. F. Shurvell, D. Lightner and R. G. Crooks, *Introduction to Organic Spectroscopy*, Macmillan Publishing Company, New York, 1987; R. D. Foust and P. C. Ford, *J. Am. Chem. Soc.*, 1972, **94**, 5686; C. A. Stein and H. Taube, *J. Am. Chem. Soc.*, 1978, **100**, 336; H. Lehmann, K. J. Schenk, G. Chapuis and A. Ludi, *J. Am. Chem. Soc.*, 1979, **101**, 6197; I. P. Evans, G. W. Everett and A. M. Sargeson, *J. Am. Chem. Soc.*, 1976, **98**, 8041.

23 M. Maruyama, H. Matsuzawa and Y. Kaizu, *Inorg. Chim. Acta*, 1995, **237**, 159; M. Bourgault, T. Renouard, B. Lognone, C. Mountassir and H. LeBozec, *Can. J. Chem.*, 1997, **75**, 318; L. S. Kelso, D. A. Reitsma and F. R. Keene, *Inorg. Chem.*, 1996, **35**, 5144.

24 J. K. M. Sanders and B. K. Hunter, *Modern NMR Spectroscopy, A Guide for Chemists*, Oxford University Press, New York, 1978; J. B. Lambert, H. F. Shurvell, D. Lightner and R. G. Crooks, *Introduction to Organic Spectroscopy*, Macmillan Publishing Company, New York, 1987.

25 R. R. Ruminski and J. D. Petersen, *Inorg. Chem.*, 1982, **21**, 3706.

26 C. Creutz, *Prog. Inorg. Chem.*, 1983, **30**, 1 and references therein.

27 A. B. P. Lever, *Inorg. Chem.*, 1990, **29**, 1271.

28 P. Bernhard, D. J. Bull, H. B Burgi. P. Osvath, A. Raselli and A. M. Sargeson, *Inorg. Chem.*, 1997, **36**, 2804; M. J. Ridd and F. R. Keene, *J. Am. Chem. Soc.*, 1981, **103**, 5733; V. L. Goedkin and D. H. Busch, *J. Am. Chem. Soc.*, 1972, **94**, 7355; P. Bernhard, D. J. Bull, H. B. Burgi. P. Osvath, A. Raselli and A. M. Sargeson, *Inorg. Chem.*, 1997, **36**, 2804; E. Jandrasics, B. Kolp, J. A. Wolny and A. von Zelewsky, *Inorg. Chim. Acta*, 1998, **272**, 153; J. C. Dabrowiak, F. V. Lovecchio and D. H. Busch, *J. Am. Chem. Soc.*, 1972, **94**, 5502; R. Arakawa, S. Mimura, G. Matsubayashi and T. Matsuo, *Inorg. Chem.*, 1996, **35**, 5725; M. A. Fox and M. T. Dulay, *Chem. Rev.*, 1993, **93**, 341; B. C. Lane, J. E. Lester and F. Basolo, *Chem. Commun.*, 1971, 1618; D. F. Mahoney and J. K. Beattie, *Inorg. Chem.*, 1973, **12**, 2561; F. R. Keene, P. A. Lay, G. E. Sneddon and G. W. Whebell, *Aust. J. Chem.*, 1993, **46**, 1763; P. Berhard and F. C. Anson, *Inorg. Chem.*, 1989, **28**, 3272; P. A. Lay, G. M. McLaughlin and A. M. Sargeson, *Aust. J. Chem.*, 1987, **40**, 1267; F. R. Keene, *Coord. Chem. Rev.*, 1999, **187**, 121.

29 P. H. Rieger, *Coord. Chem. Rev.*, 1994, **135/136**, 203 and references therein; A. R. Chakravarty and A. Chakravorty, *Inorg. Chem.*, 1981, **20**, 3138; N. Bag, G. K. Lahiri and A. Chakravorty, *J. Chem. Soc., Dalton Trans.*, 1990, 1557; G. K. Lahiri, S. Bhattacharya, M. Mukherjee, A. K. Mukherjee and A. Chakravorty, *Inorg. Chem.*, 1987, **26**, 3359; G. K. Lahiri, S. Bhattacharya, B. K. Ghosh and A. Chakravorty, *Inorg. Chem.*, 1987, **26**, 4324; H. K. Gupta and S. Dikshit, *Polyhedron*, 1987, **6**, 1009; N. S. Hush and A. Edgar, *Chem. Phys. Lett.*, 1980, **69**, 128; K. Matsumoto, T. Matsumoto, M. Kawano, H. Ohnuki, Y. Shichi, T. Nishide and T. Sato, *J. Am. Chem. Soc.*, 1996, **118**, 3597.

30 C. Joachim, S. P. Launay and S. Woitellier, *Chem. Phys.*, 1990, **147**, 131; J. P. Collin and J. P. Sauvage, *J. Am. Chem. Soc.*, 1998, **120**, 3717.

31 A. B. P. Lever, work in progress.

32 A. Freda, undergraduate thesis project.

Paper 9/02850A